Neuron
Primer

Imaging Calcium in Neurons

Christine Grienberger[1] and Arthur Konnerth[1,*]
[1]Institute of Neuroscience, Technical University Munich, Biedersteinerstr. 29, 80802 Munich, Germany
*Correspondence: arthur.konnerth@lrz.tum.de
DOI 10.1016/j.neuron.2012.02.011

Calcium ions generate versatile intracellular signals that control key functions in all types of neurons. Imaging calcium in neurons is particularly important because calcium signals exert their highly specific functions in well-defined cellular subcompartments. In this Primer, we briefly review the general mechanisms of neuronal calcium signaling. We then introduce the calcium imaging devices, including confocal and two-photon microscopy as well as miniaturized devices that are used in freely moving animals. We provide an overview of the classical chemical fluorescent calcium indicators and of the protein-based genetically encoded calcium indicators. Using application examples, we introduce new developments in the field, such as calcium imaging in awake, behaving animals and the use of calcium imaging for mapping single spine sensory inputs in cortical neurons in vivo. We conclude by providing an outlook on the prospects of calcium imaging for the analysis of neuronal signaling and plasticity in various animal models.

Introduction

Calcium ions generate versatile intracellular signals that determine a large variety of functions in virtually every cell type in biological organisms (Berridge et al., 2000), including the control of heart muscle cell contraction (e.g., Dulhunty, 2006) as well as the regulation of vital aspects of the entire cell cycle, from cell proliferation to cell death (Lu and Means, 1993; Orrenius et al., 2003). In the nervous system, calcium ions preserve and, perhaps, even extend their high degree of versatility because of the complex morphology of neurons. In presynaptic terminals, calcium influx triggers exocytosis of neurotransmitter-containing synaptic vesicles (for review, see Neher and Sakaba, 2008). Postsynaptically, a transient rise of the calcium level in dendritic spines is essential for the induction of activity-dependent synaptic plasticity (Zucker, 1999). In another cellular subcompartment, the nucleus, calcium signals can regulate gene transcription (Lyons and West, 2011). Importantly, intracellular calcium signals regulate processes that operate over a wide time range, from neurotransmitter release at the microsecond scale to gene transcription, which lasts for minutes and hours (Berridge et al., 2003). Thus, the time course, the amplitude, and, most notably, the local action site in well-defined cellular subcompartments are essential determinants for the function of intracellular calcium signals. Therefore, not surprisingly, the direct investigation of the plethora of diverse neuronal calcium functions benefited enormously from the development of techniques allowing the visualization and quantitative estimation of the intracellular calcium signals.

Historically, the development of calcium imaging involved two parallel processes: the development and the continuous improvement of calcium sensors, and the development and the implementation of the appropriate instrumentation. Among the first calcium indicators used for monitoring the dynamics of cellular calcium signaling were bioluminescent calcium-binding photoproteins, such as aequorin (Ashley and Ridgway, 1968; Shimomura et al., 1962). A next class of calcium indicators is represented by the synthetic compound arsenazo III, an absorbance dye that changes its absorption spectrum as a function of bound calcium (Brown et al., 1975). While aequorin and arsenazo III provided important early insights into the calcium-dependent regulation of neuronal processes (Hallett and Carbone, 1972; Llinás and Nicholson, 1975; Stinnakre and Tauc, 1973), their implementation and use was often tedious, mostly because of problems with dye delivery. A true breakthrough was then the development of more sensitive and versatile fluorescent calcium indicators and buffers by Roger Tsien and colleagues (Tsien, 1980). These indicators were the result of the hybridization of highly calcium-selective chelators like EGTA or BAPTA with a fluorescent chromophore. The first generation of fluorescent calcium indicators consisted of quin-2, fura-2, indo-1, and fluo-3. Quin-2 is excited by ultraviolet light (339 nm) and was the first dye of this group to be used in biological experiments (Pozzan et al., 1982; Tsien et al., 1982). Quin-2, however, is not particularly bright and needs to be used at high intracellular concentrations to overcome cellular autofluorescence (Tsien, 1989). Instead, another dye of that family, namely fura-2 (Grynkiewicz et al., 1985), is in many ways superior to quin-2 and became very popular among neuroscientists. Fura-2 is usually excited at 350 and/or 380 nm and shows calcium-dependent fluorescence changes that are significantly larger than the ones produced by quin-2. Furthermore, fura-2 is particularly useful because it allows more quantitative calcium measurements involving the ratioing of the signals obtained with alternating the excitation wavelengths (Neher, 1995). Over the years, many more calcium indicators with a wide range of excitation spectra and affinities for calcium have been introduced. These include, among others, the Oregon Green BAPTA and fluo-4 dye families (Paredes et al., 2008). These dyes are widely used in neuroscience because they are relatively easy to implement and provide large signal-to-noise ratios. An important next breakthrough, again from the laboratory of Roger Tsien (Miyawaki et al., 1997), was the introduction of protein-based genetically encoded calcium indicators (GECIs). While the early types of GECIs had somewhat limited areas of application because of their slow response kinetics and low signal-to-noise ratios,

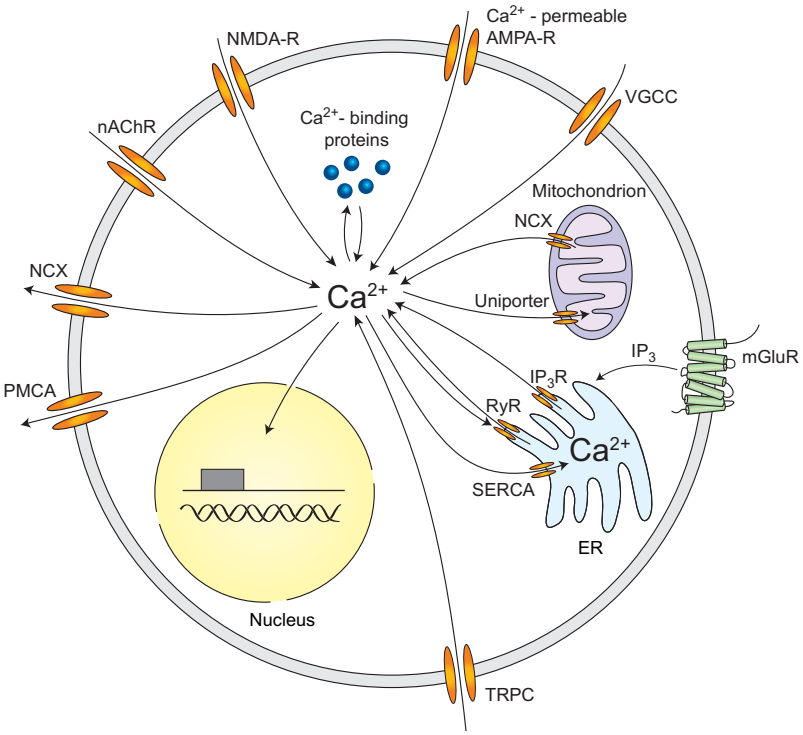

Figure 1. Neuronal Calcium Signaling
Sources of calcium influx are calcium-permeable α-amino-3-hydroxy-5-methyl-4-isoxazolepropionic acid (AMPA) and N-methyl-D-aspartate (NMDA) glutamate-type receptors, voltage-gated calcium channels (VGCC), nicotinic acetylcholine receptors (nAChR), and transient receptor potential type C (TRPC) channels. Calcium release from internal stores is mediated by inositol trisphosphate receptors (IP_3R) and ryanodine receptors (RyR). Inositol trisphosphate can be generated by metabotropic glutamate receptors (mGluR). Calcium efflux is mediated by the plasma membrane calcium ATPase (PMCA), the sodium-calcium exchanger (NCX), and the sarco-/endoplasmic reticulum calcium ATPase (SERCA). Also the mitochondria are important for neuronal calcium homeostasis

there had been tremendous progress in recent years (for review, see Looger and Griesbeck, 2011; Rochefort et al., 2008).

The development of the fluorescent indicators was paralleled by the development of new imaging instrumentation. This included the implementation of video imaging (Smith and Augustine, 1988; Swandulla et al., 1991), of CCD cameras (Connor, 1986; Lasser-Ross et al., 1991), and of high-speed confocal microscopy (Eilers et al., 1995) for calcium imaging. The high signal strength of the fluorescent probes in combination with these emerging technologies allowed for real-time fluorescence observations of biological processes at the single-cell level. A major advance was in the early 1990s the introduction of two-photon microscopy by Winfried Denk and colleagues (Denk et al., 1990) and its use for calcium imaging in the nervous system (Yuste and Denk, 1995). Two-photon imaging has revolutionized the field of calcium imaging (Helmchen and Denk, 2005; Svoboda and Yasuda, 2006) and is now used worldwide in many laboratories. In this Primer, after providing an introduction to neuronal calcium signaling, we describe what we believe to be the most important features for the application of calcium imaging in the nervous system. This includes the selection of the appropriate calcium indicator, the different dye-loading techniques, and the most popular imaging devices used for in vitro and in vivo calcium imaging. We focus on experiments performed in rodents as animal models, mostly because of their widespread use in the calcium imaging community.

Neuronal Calcium Signaling

Calcium is an essential intracellular messenger in mammalian neurons. At rest, most neurons have an intracellular calcium concentration of about 50–100 nM that can rise transiently during electrical activity to levels that are ten to 100 times higher (Berridge et al., 2000). Figure 1 summarizes some of the most important sources of neuronal calcium signaling, without taking into account their spatial organization into the different cellular subcompartments, such as dendritic arbor, cell body, or presynaptic terminal. At any given moment, the cytosolic calcium concentration is determined by the balance between calcium influx and efflux as well as by the exchange of calcium with internal stores. In addition, calcium-binding proteins such as parvalbumin, calbindin-D28k, or calretinin, acting as calcium buffers, determine the dynamics of free calcium inside neurons (Schwaller, 2010). Importantly, only free calcium ions are biologically active. There are multiple mechanisms underlying the calcium influx from the extracellular space, including voltage-gated calcium channels, ionotropic glutamate receptors, nicotinic acetylcholine receptors (nAChR), and transient receptor potential type C (TRPC) channels (Fucile, 2004; Higley and Sabatini, 2008; Ramsey et al., 2006). Calcium ions are removed from the cytosol by the plasma membrane calcium ATPase (PMCA) and the sodium-calcium exchanger (NCX) (Berridge et al., 2003). Calcium release from internal stores, mostly the endoplasmic reticulum (ER), is mediated by inositol trisphosphate receptors and ryanodine receptors (Berridge, 1998). Inositol trisphosphate can be generated in neurons, for example, by the activation of metabotropic glutamate receptors (Niswender and Conn, 2010). The high calcium level inside the ER is maintained by the sarco-/endoplasmic reticulum calcium ATPase (SERCA) that transports calcium ions from the cytosol to the lumen of the ER. In addition to the ER, mitochondria are also important for neuronal calcium homeostasis. Mitochondria can act as calcium buffers by taking calcium up during cytosolic calcium elevations through the calcium uniporter and then releasing it back to the cytosol slowly through sodium-calcium exchange (Duchen, 1999). In the following we describe in more detail some of the main contributors to neuronal calcium signaling.

Voltage-Gated Calcium Channels

VGCCs comprise a broad class of channels with a high selectivity for calcium ions and a wide variety of voltage-dependent

activation and inactivation features. Based on their threshold of voltage-dependent activation they are generally categorized into high- (HVA) and low-voltage-activated (LVA) channels (Catterall, 2000). HVA channels can be further subdivided based on their biophysical, pharmacological, and molecular features. They are traditionally classified as L-, P/Q-, N-, and R-type calcium channels. Which class of VGCC is present in a given neuron depends on the cell type and also on the cellular subcompartment. For example, T-type LVA channels are highly expressed in thalamic neurons (Coulter et al., 1989), while P-type channels are highly abundant in cerebellar Purkinje neurons (Usowicz et al., 1992). L-type and predominantly R-type VGCCs are abundant in dendritic spines of pyramidal neurons (Bloodgood and Sabatini, 2007b; Hoogland and Saggau, 2004; Yasuda et al., 2003), while P/Q- and N-type channels are found in many nerve terminals (Catterall, 2000; Plant et al., 1998). In the dendrites and spines of most central neurons, VGCCs are effectively activated by backpropagation of action potentials (Spruston et al., 1995; Waters et al., 2005) and by synaptically mediated depolarization of dendritic spines (Bloodgood and Sabatini, 2007b; Reid et al., 2001). As the recording of somatic calcium signals is widely used for the monitoring of action potential activity in vitro (Mao et al., 2001) and in vivo (Stosiek et al., 2003), it is important to note that here VGCCs are the main determinant of these signals. An important functional role of somatic calcium signals is the induction of gene transcription (Lyons and West, 2011).

N-Methyl-D-Aspartate Receptors

NMDA receptors are ionotropic glutamate receptors and mediate a major part of the postsynaptic calcium influx in the dendritic spines of various neuronal cell types, such as pyramidal neurons of the hippocampus (Bloodgood and Sabatini, 2007b; Kovalchuk et al., 2000; Sabatini et al., 2002; Yuste et al., 1999) and cortex (Koester and Sakmann, 1998; Nevian and Sakmann, 2006). This rise in spine calcium concentration is particularly important for the long-term modification of synaptic strength (Zucker, 1999). NMDA receptor channels are nonspecific cation channels that are permeable for sodium, potassium, and calcium ions. The fraction of calcium ions contributing to the total cation current through NMDA receptor channels is about 6%–12% (Burnashev et al., 1995; Garaschuk et al., 1996; Rogers and Dani, 1995; Schneggenburger et al., 1993). The specific properties of NMDA receptors are determined by the subunit composition, the phosphorylation status of the receptor, and, importantly, the membrane potential of the neuron. NMDA receptors are heteromers of the subunit NR1 in combination with NR2 subunits, like NR2A or NR2B (Bloodgood and Sabatini, 2007a). In CA1 hippocampal neurons, dendritic spines express preferentially either the NR2A or the NR2B subunits and, in a given neuron, the contribution of NR2A- or NR2B-mediated calcium influx to the spine calcium signal is variable among the different dendritic spines (Sobczyk et al., 2005). Another factor that determines the permeability for calcium ions is the phosphorylation status of the NMDA receptors. Thus, the permeability is enhanced by increased phosphorylation whereas dephosphorylation decreases calcium permeability (Skeberdis et al., 2006; Sobczyk and Svoboda, 2007). Finally, a critical modulator of NMDA receptor function is the membrane potential as it determines the efficacy of the voltage-dependent block of NMDA receptors by magnesium (Mayer et al., 1984; Nowak et al., 1984). The NMDA receptor-dependent ionic current increases as a function of increasing neuronal depolarization from the resting membrane potential.

Calcium-Permeable α-Amino-3-Hydroxy-5-Methyl-4-Isoxazolepropionic Acid Receptors

Calcium-permeable AMPA receptors are another class of ionotropic glutamate receptors. They are found in many forms of aspiny GABAergic neurons and characterized by the relative lack of the GluR2 receptor subunit (Jonas et al., 1994). GluR2-lacking AMPA receptors are permeable for sodium, calcium, potassium, but also zinc ions (Liu and Zukin, 2007). They exhibit fast gating kinetics (Geiger et al., 1995) and their inwardly rectifying I-V relationship arises from a voltage-dependent block due to intramolecular polyamines (Bowie and Mayer, 1995; Koh et al., 1995). The subunit composition varies in a synapse-specific manner within individual neurons (Tóth and McBain, 1998). This feature enables individual neurons to produce different types of responses to distinct synaptic inputs. Importantly, the presence of GluR2-containing and GluR2-lacking AMPA receptors is not static, but is highly regulated, particularly in response to neuronal activity (Liu and Cull-Candy, 2000). Thus, permeability of AMPA receptors to calcium is dynamic within a given neuron and can therefore contribute to synaptic plasticity mechanisms in aspiny neurons. For example, tetanic stimulation of synaptic inputs from excitatory neurons onto amygdala interneurons produces long-term potentiation (LTP) of the excitatory postsynaptic currents, a form of plasticity thought to be an important cellular mechanism for fear conditioning (Mahanty and Sah, 1998). This potentiation was independent of NMDA receptors and thus, in these aspiny neurons, calcium-permeable AMPA receptors probably mediate a major component of calcium signaling during LTP induction. In another type of aspiny neurons, namely, neocortical GABAergic cells, Goldberg et al. (2003) used two-photon calcium imaging to demonstrate that activation of single synapses creates highly localized dendritic calcium signals. The characteristics of this calcium signal are determined by the fast kinetics of calcium-permeable AMPA receptors, the fast local extrusion through the sodium-calcium-exchanger, and the buffering by calcium-binding proteins, such as parvalbumin (Goldberg et al., 2003). Thus, the authors concluded that the expression of calcium-permeable AMPA receptors in spine-lacking neurons might enable calcium signal compartmentalization in response to single synapse activation, somewhat similarly to synapses located on dendritic spines in excitatory neurons, a feature that may have important consequences for neuronal processing in aspiny neurons. In pyramidal neurons, calcium-permeable AMPA receptors have also been shown to be involved in some forms of synaptic calcium signaling. For example, sensory activation can promote an increase in calcium that is mediated by GluR2-lacking AMPA receptors at neocortical layer 4-layer 2/3 excitatory synapses. This calcium signal may represent an alternate source for activity-dependent calcium entry, facilitating the initiation of synaptic plasticity (Clem and Barth, 2006).

Metabotropic Glutamate Receptors

mGluRs are 7-transmembrane G protein-coupled receptors that are broadly distributed within the nervous system (Ferraguti and

Shigemoto, 2006). They are classified in group I, II, and III mGluRs, are expressed in a cell-type-specific fashion, and exert diverse physiological roles (Lüscher and Huber, 2010). The receptor classes differ in their downstream signaling mechanisms; for example, group I mGluRs are coupled to the G_q protein (Wettschureck and Offermanns, 2005). In cerebellar Purkinje neurons, the mGluR1 subtype of this group mediates both an increase in intracellular calcium as well as a TRPC3-dependent inward current (Hartmann et al., 2008). Upon activation of mGluR1, phospholipase C mediates the generation of IP_3, which binds to receptors in the ER and induces calcium release (Niswender and Conn, 2010).

Calcium Release from Internal Stores

Calcium release from internal stores is best known to occur from the ER through inositol trisphosphate receptors (IP_3Rs) and ryanodine receptors (RyRs) but may involve also other intracellular organelles (Rizzuto and Pozzan, 2006). Calcium signals resulting from calcium release from internal stores have been found in various types of neurons at different developmental stages (e.g., Llano et al., 2000; Lohmann et al., 2005; Manita and Ross, 2009). While IP_3-mediated calcium release is mostly triggered by neurotransmitters such as glutamate (see above), RyRs can be activated by elevations of the cytosolic calcium concentration. This RyR-mediated process of calcium-induced calcium release can contribute, for example, to the amplification of the calcium influx generated by action potential firing in neurons (Kano et al., 1995; Tsien and Tsien, 1990). Both IP_3Rs and RyRs are regulated by various intracellular factors, perhaps most importantly by calcium itself (Berridge, 1993). The regulatory action through calcium applies from both the lumenal or cytosolic side of the channels. This calcium dependence establishes a feedback loop coordinating calcium influx from the internal stores into the cytosol and plays, in the case of IP_3Rs, an essential role for synaptically evoked dendritic calcium waves in neocortical and other types of neurons (Larkum et al., 2003; Nakamura et al., 1999).

A major challenge in the analysis of the various sources of neuronal calcium signaling is that they are generally not active one at a time, but have overlapping activities with strong interactions. For example, during strong synaptic activity calcium influx through both NMDA receptors and VGCCs in the dendrites and spines of CA1 hippocampal neurons sum up nonlinearly and their combined signals acts as a coincidence detector between pre- and postsynaptic activity (Yuste and Denk, 1995). Similarly, in cerebellar Purkinje cells, the pairing of climbing fiber activity with parallel fiber bursts triggers dendritic calcium signals that are largest when activation of parallel fibers precedes the climbing fiber activation by a certain time window (Wang et al., 2000). In view of these complexities, calcium imaging is often indispensable for the dissection of the specific signaling mechanisms in neurons.

Calcium Indicators

Figure 2A describes the mode of action of the bioluminescent calcium indicator *aequorin*, derived from marine organisms, such as the luminescent jellyfish aequorea victoria (Shimomura et al., 1962). It is composed of the apoprotein apoaequorin and a noncovalently bound chromophore, a combination of coelenterazine and molecular oxygen (Ohmiya and Hirano, 1996). It contains three calcium-binding sites (Head et al., 2000). Upon binding of calcium ions, the protein undergoes a conformational change resulting in the oxidation of coelenterazine to coelenteramide and in the emission of a photon (about 470 nm wavelength) due to the decay of coelenteramide from the excited to the ground state (Ohmiya and Hirano, 1996). The rate of this reaction depends on the cytosolic calcium concentration (Cobbold and Rink, 1987). Importantly, aequorin is characterized by a high signal-to-noise ratio and a wide dynamic range being able to monitor changes in the cytosolic calcium concentration from 10^{-7} to 10^{-3} M (Bakayan et al., 2011; Brini, 2008). Bioluminescent recordings of calcium signals using aequorin do not require external illumination, thus avoiding problems such as phototoxicity, photobleaching, autofluorescence, and undesirable stimulation of photobiological processes (Xu et al., 2007). However, each molecule performs only one emission cycle and, unfortunately, the recharging process with the coelenterazine is relatively slow (Shimomura et al., 1993). Moreover, as the extracted form of aequorin cannot penetrate the plasma membrane of intact cells, it needs to be loaded into single cells by means of a micropipette (Chiesa et al., 2001). The cloning and sequence analysis of the aequorin cDNA has partially overcome this problem by enabling apoaequorin expression in a wide variety of cell types and from defined intracellular compartments (Inouye et al., 1985; Rizzuto et al., 1992). However, all these applications using expression of the apoprotein require exogenous supplementation of coelenterazine (Shimomura, 1997). In general, aequorin-based recording of calcium signals suffers from low quantum yield and low protein stability (Brini, 2008). In an attempt to increase the quantum yield, aequorin has been combined with different fluorescent proteins (Bakayan et al., 2011; Baubet et al., 2000; Martin et al., 2007; Rogers et al., 2005).

Figure 2B shows the structure of *fura-2*, a representative example for the fluorescent chemical (or synthetic) calcium indicators (Grynkiewicz et al., 1985). As already mentioned, fura-2 is a combination of calcium chelator and fluorophore. It is excitable by ultraviolet light (e.g., 350/380 nm) and its emission peak is between 505 and 520 nm (Tsien, 1989). The binding of calcium ions causes intramolecular conformational changes that lead to a change in the emitted fluorescence. With one-photon excitation, fura-2 has the advantage that it can be used with dual wavelength excitation, allowing the quantitative determination of the calcium concentration in a neuron of interest independently of the intracellular dye concentration (Tsien et al., 1985). Another advantage of fura-2 is that it has a good cross-section for two-photon calcium imaging (Wokosin et al., 2004; Xu et al., 1996). However, because of the broad absorption spectrum in conditions of two-photon excitation, ratiometric recording is not feasible. Instead, fura-2 and GFP labeling can be readily combined because of their well-separated absorption peaks. For example, fura-2 has been successfully used for two-photon calcium imaging in GFP-labeled interneurons (Sohya et al., 2007). While fura-2 emitted fluorescence decreases upon calcium elevations in conditions of two-photon imaging, the fluorescence of other indicators, like Oregon Green BAPTA and fluo, increases with calcium elevations inside cells. Perhaps

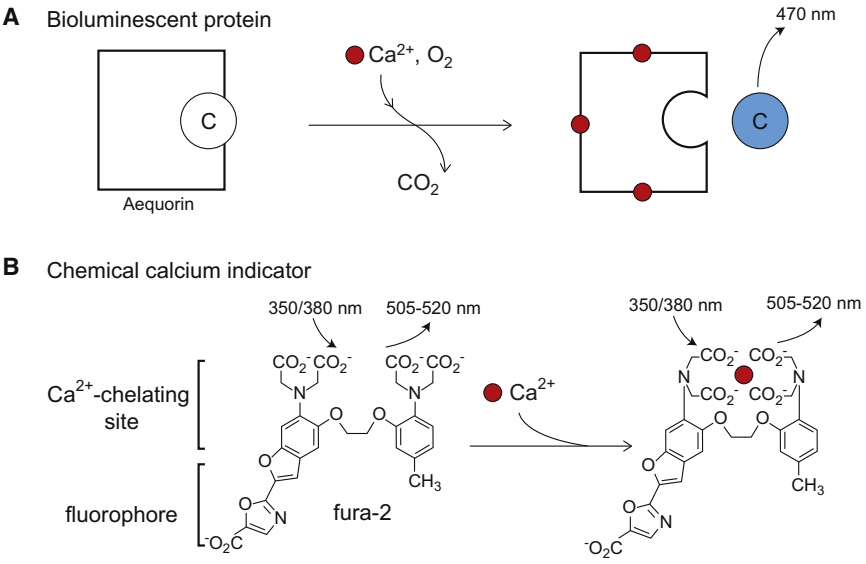

Figure 2. Calcium Indicators

(A) Bioluminescent protein. Binding of calcium ions to aequorin leads to the oxidation of the prosthetic group coelenterazine (C, left side) to colenteramide (C, right side). Colenteramide relaxes to the ground state while emitting a photon of 470 nm.

(B) Chemical calcium indicator. Fura-2 is excitable by ultraviolet light (e.g., 350/380 nm) and its emission peak is between 505 and 520 nm. The binding of calcium ions by fura-2 leads to changes in the emitted fluorescence.

(C) FRET-based genetically encoded calcium indicator (GECI). After binding of calcium ions to yellow cameleon 3.60 the two fluorescent proteins, ECFP (donor) and Venus (acceptor), approach. This enables Förster resonance energy transfer (FRET) and thus, the blue fluorescence of 480 nm decreases, whereas the fluorescence of 530 nm increases.

(D) Single-fluorophore genetically encoded calcium indicator (GECI). After binding of calcium to GCaMP conformational intramolecular changes lead to an increase in the emitted fluorescence of 515 nm.

these indicators became therefore quite popular for more noisy recording conditions like those present in vivo (e.g., Sato et al., 2007; Stosiek et al., 2003). Another major advantage of the chemical calcium indicators is that they exist in a membrane-permeable as well as in a membrane-impermeable form enabling their use in combination with a variety of different loading techniques (see section on dye-loading approaches) (Helmchen and Waters, 2002). Finally, these indicators are available at different calcium affinities and different spectral properties, allowing their simultaneous use (for overview of dye properties, see Johnson and Spence, 2010).

Genetically encoded calcium indicators (GECIs) come in two flavors, namely, those involving Förster resonance energy transfer (FRET) (Figure 2C) and the single-fluorophore ones (Figure 2D). For the illustration of the FRET-based GECIs we selected as a representative *Yellow Cameleon (YC) 3.60* (Nagai et al., 2004) (Figure 2C). FRET refers to a form of nonradiative energy transfer between an excited donor fluorophore and an acceptor fluorophore (Jares-Erijman and Jovin, 2003). Their distance has to be less than 10 nm in order to enable FRET. YC 3.60 consists of two fluorescent proteins and is part of the cameleon family of GECIs (Miyawaki et al., 1999; Miyawaki et al., 1997). It is composed of the enhanced cyan fluorescent protein (ECFP) as donor and the circularly permuted Venus protein as acceptor. These two proteins are connected by a linker sequence that consists of the calcium-binding protein calmodulin and the calmodulin-binding peptide M13 (Nagai et al., 2004). In the absence of calcium ions, the emission is dominated by the blue ECFP fluorescence (480 nm). Upon calcium binding, intramolecular conformational changes lead to reduction of the spatial distance between the two fluorescent proteins. Thus, the Venus protein is excited due to the occurrence of FRET and emits photons of about 530 nm. In practice, the blue fluorescence decreases, whereas the yellow fluorescence increases. The calcium signal is expressed as a ratio between the Venus and the ECFP fluorescence. To avoid possible interactions of calmodulin with endogenous binding partners, two different approaches were taken. In D3cpV-type GECIs, the calmodulin-M13-binding interfaces were mutated to strongly reduce the interactions with cellular targets (Palmer et al., 2006; Wallace et al., 2008). In another type of FRET-based calcium indicators, calmodulin is replaced by troponin C variants (Heim et al., 2007; Heim and Griesbeck, 2004; Mank et al., 2006; Mank et al., 2008). Troponin C is the calcium-binding protein in the cardiac and skeletal muscle cells and as such it does not have endogenous binding partners in neurons.

A prime representative of the single-fluorophore GECIs is the *GCaMP* family (Figure 2D) that is increasingly used for calcium

Table 1. Frequently Used Fluorometric Calcium Indicators

Name	Kd (nM)	Examples of In Vivo Applications	Representative References
Chemical Calcium Indicators			
Oregon Green BAPTA-1	170	Mouse neocortex, mouse hippocampus, mouse olfactory bulb, rat neocortex, rat cerebellum, ferret neocortex, cat neocortex, zebrafish	Dombeck et al., 2010; Sullivan et al., 2005; Ohki et al., 2005; Li et al., 2008; Greenberg et al., 2008; Rochefort et al., 2011; Sumbre et al., 2008; Wachowiak et al., 2004
Calcium Green-1	190	Mouse neocortex, mouse olfactory bulb, honeybee, turtle, zebrafish, rat neocortex	Dombeck et al., 2009; Oka et al., 2006; Galizia et al., 1999; Wachowiak et al., 2002; Brustein et al., 2003; Svoboda et al., 1997
Fura-2	140	Mouse neocortex	Sohya et al., 2007
Indo-1	230	Mouse neocortex	Stosiek et al., 2003
Fluo-4	345	Mouse neocortex, Xenopus larvae	Sato et al., 2007; Demarque and Spitzer, 2010
Rhod-2	570	Mouse neocortex, Zebrafish	Takano et al., 2006; Yaksi et al., 2009
X-rhod-1	700	Mouse neocortex	Nagayama et al., 2007
Genetically Encoded Calcium Indicators			
Camgaroo 1		Drosophila	Yu et al., 2003
Camgaroo 2		Drosophila, mouse olfactory bulb	Yu et al., 2003; Hasan et al., 2004
Inverse pericam	200	Zebrafish, mouse olfactory bulb	Hasan et al., 2004; Li et al., 2005
GCaMP 2	840	Mouse olfactory bulb, mouse cerebellum	Fletcher et al., 2009; Díez-García et al., 2005
GCaMP 3	660	Mouse neocortex, mouse hippocampus, Drosophila, C. elegans	Tian et al., 2009; Dombeck et al., 2010; Seelig et al., 2010; Tian et al., 2009
Yellow Cameleon 3.6	250	Mouse neocortex	Lütcke et al., 2010
Yellow Cameleon Nano	15–50	Zebrafish	Horikawa et al., 2010
D3cpV	600	Mouse neocortex	Wallace et al., 2008
TN-XL	2200	Drosophila, macaque	Mank et al., 2006; Heider et al., 2010
TN-L15	710	Mouse neocortex	Heim et al., 2007
TN-XXL	800	Drosophila, mouse neocortex	Mank et al., 2008; Mank et al., 2008

K_d dissociation constant in nM. K_d values taken from The Molecular Probes Handbook (chemical calcium indicators), Nagai et al., 2001 (Pericam), Tian et al., 2009 (GCaMP), Nagai et al., 2004 (YC 3.6), Horikawa et al., 2010 (YC-Nano), Palmer et al., 2006 (D3cpv), and Mank et al., 2008 (TN-based).

imaging in in vivo conditions (Chalasani et al., 2007; Dombeck et al., 2010; Fletcher et al., 2009; Wang et al., 2003). GCaMPs consist of a circularly permuted enhanced green fluorescent protein (EGFP), which is flanked on one side by the calcium-binding protein calmodulin and on the other side by the calmodulin-binding peptide M13 (Nakai et al., 2001). In the presence of calcium, calmodulin-M13 interactions elicit conformational changes in the fluorophore environment that lead to an increase in the emitted fluorescence (Nakai et al., 2001; Tian et al., 2009). Recently, after elucidating the structure of the GCaMP2, GCaMP3 was developed by protein engineering. It is improved concerning its signal-to-noise ratio, dynamic range, and response kinetics but it does not show reliable single action-potential-associated calcium signals (Tian et al., 2009; Yamada et al., 2011).

Table 1 gives an overview of the most widely used calcium indicators, including some representative references and examples of applications. As a final note, it is important to remain aware of the fact that calcium indicators measure changes in the cytosolic free calcium concentration. Free calcium ions are in equilibrium with the calcium ions that are bound to endogenous calcium buffers, such as parvalbumin, calbindin-D28k, and calretinin (Baimbridge et al., 1992). In calcium imaging experiments, the calcium indicators, except for aequorin, act as exogenous calcium buffer and thereby contribute to the total amount of cellular calcium buffer molecules (Helmchen et al., 1996). Therefore, adding calcium indicator will change the intracellular calcium dynamics (Neher and Augustine, 1992). In its simplest case, this perturbation is described by the "single-compartment model," which takes into account the endogenous calcium-binding proteins and the exogenous calcium indicator (Helmchen et al., 1996; Regehr and Tank, 1994). It is useful because it allows the estimation of the unperturbed calcium dynamics within the cytosol. For example, it has been successfully used for describing calcium dynamics in dendrites (Regehr and Tank, 1994). Notably, calcium indicators differ in their affinities for calcium (Mank and Griesbeck, 2008; Paredes et al., 2008) (Table 1). This is reflected in the dissociation constant (K_d) that describes the likelihood that a complex of indicator and calcium ion will separate. The K_d has a molar unit and corresponds to the calcium concentration at which half of the indicator molecules are bound to calcium. There are low- (e.g., fluo-5N) and high-affinity (e.g., Oregon Green BAPTA-1) calcium indicators. The measured K_d value is dependent on many parameters, including pH, temperature, and the presence of magnesium (Oliver et al., 2000). Consequently, it might vary between in vitro and in vivo condition. When designing an experiment, choosing the appropriate indicator in the appropriate

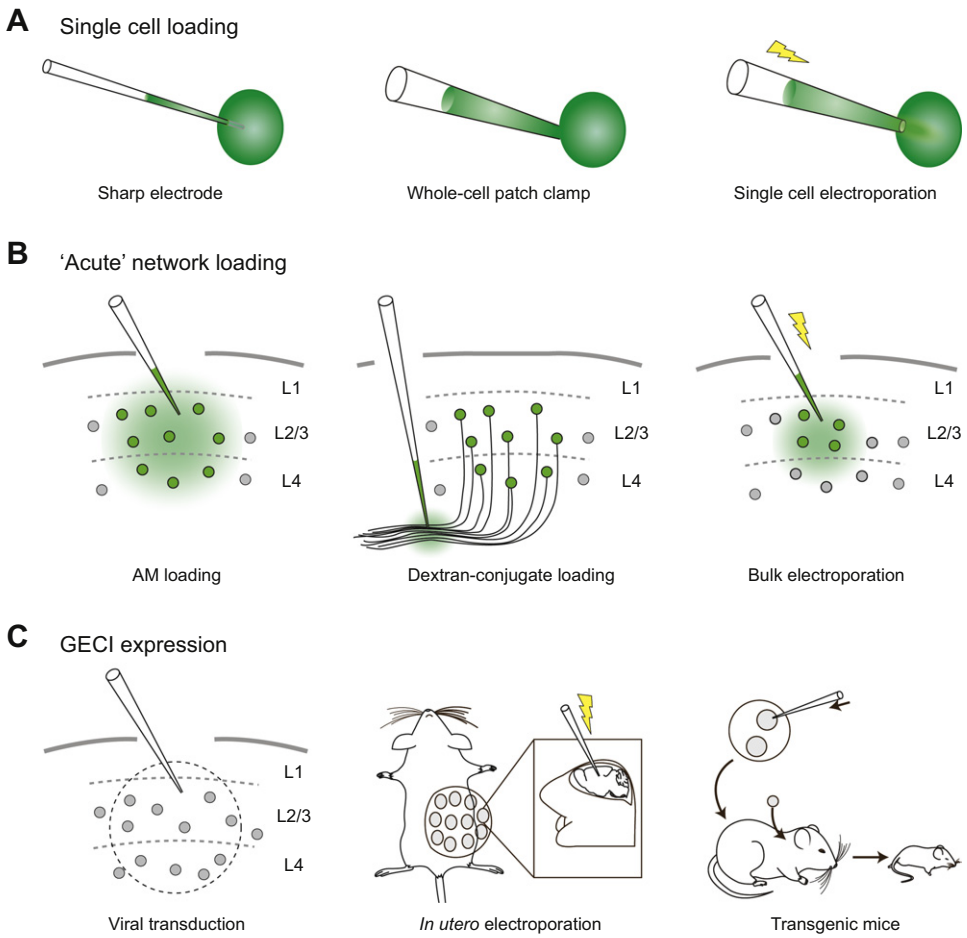

Figure 3. Dye-Loading Approaches

(A) Single-cell loading by sharp electode impalement (left panel), whole-cell patch-clamp configuration (middle panel), and single-cell electroporation (right panel). Note that these approaches can be used for loading of chemical and genetically encoded calcium indicators.

(B) "Acute" network loading. Many neurons are labeled simultaneously by acetoxymethyl ester (AM) loading (left panel), by loading with dextran-conjugated dye (middle panel), and by bulk electroporation (left panel).

(C) Expression of genetically encoded calcium indicators (GECI) by viral transduction (left panel), in utero electroporation (middle panel), and generation of transgenic mouse lines (right panel).

concentration is essential for the interpretation of the results. This decision should be guided by the scientific goals of the measurement and by the cells of interest. For example, fluorescent signals recorded with low-affinity indicators, which add little buffer capacity to the cell, reflect more accurately the change in the free cytosolic calcium concentration. These calcium signals will have faster rise and decay times than those recorded with high-affinity indicators (Helmchen et al., 1997). However, the use of low-affinity calcium indicators is limited by the need for sufficient sensitivity. This problem becomes increasingly significant when imaging in the noisy in vivo condition and when imaging small structures, such as dendritic spines. In these conditions, high-affinity calcium dyes remain, with all their limitations, the indicators of choice. Fortunately, calcium indicators with different properties can often be easily used complementarily in an experimental series. The new developments will certainly add up to our ability of deciphering the highly complex mechanisms of neuronal signaling in the intact nervous system.

Dye-Loading Approaches

The loading of calcium indicators into neurons depends on the type of calcium indicator, the biological preparation, and the specific scientific question. Figure 3A illustrates the three most widely used approaches for dye loading of individual neurons. In the early imaging experiments, chemical calcium dyes were delivered through sharp microelectrodes both in vitro (Jaffe et al., 1992) and in vivo (Svoboda et al., 1997) (Figure 3A, left panel). In more recent years, dye delivery through whole-cell patch-clamp micropipettes became the standard procedure for single-cell dye loading for many applications (Figure 3A, middle panel) (Eilers and Konnerth, 2009; Margrie et al., 2002). A particularly useful variant of this method involves in vivo whole-cell recordings that are performed under visual guidance using two-photon imaging by applying the "shadow patching" technique (Jia et al., 2011; Kitamura et al., 2008). This approach can be combined with the targeting of genetically identified cells expressing a fluorescent marker protein (Margrie et al., 2003).

Other attractive and relatively easy-to-use single-cell approaches are the targeted electroporation (Judkewitz et al., 2009; Kitamura et al., 2008; Nevian and Helmchen, 2007) or single-cell bolus loading (Helmchen et al., 1996). After approaching the soma of the target neuron with a micropipette in the electroporation experiments (Figure 3A, right panel), a few current pulses of appropriate polarity mediate dye delivery to the cell. This approach relies on two distinct mechanisms (for review, see De Vry et al., 2010). First, the electrical current disrupts the integrity of the cellular plasma membrane for a short period of time causing the transient formation of pores through which the dye molecules diffuse into the cell. Second, the current "pushes" the charged indicator molecules out of the pipette into the cell of interest. Importantly, this approach can be used for chemical calcium indicators as well as for DNA encoding for GECIs. A limitation of this method is that, because of the absence of the recording whole-cell microelectrode, the functional status of the neurons is not entirely clear. This can be overcome by combining electroporation of single cells with the cell-attached recordings involving the use of a second, fresh micropipette (Chen et al., 2010).

Single-cell calcium imaging is widely used for the analysis of basic mechanisms of calcium signaling in neurons and for the functional analysis of dendrites and spines and calcium signaling in terminals (for specific examples and application protocols see Helmchen and Konnerth, 2011). However, calcium imaging is also widely used for the monitoring of activity in local populations of interconnected neurons. Early application examples include the analyses of the circuitry of the cortex (Garaschuk et al., 2000; Yuste and Katz, 1991; Yuste et al., 1992), the hippocampus (Garaschuk et al., 1998), and the retina (Feller et al., 1996). This technique has also been successfully applied to identify synaptically connected neurons (Aaron and Yuste, 2006; Bonifazi et al., 2009; Kozloski et al., 2001). Furthermore, it has been used to analyze pathological forms of network activity, such as epileptiform events (Badea et al., 2001; Trevelyan et al., 2006). Here we focus on three widely used approaches for dye loading of neuronal populations in intact tissues. Figure 3B (left panel) illustrates an approach for the targeted bulk dye loading of membrane-permeable acetoxymethyl (AM) ester calcium dyes (Grynkiewicz et al., 1985) involving multicell bolus loading (MCBL) (Stosiek et al., 2003). This simple method consists of the injection of an AM calcium dye, for example Oregon Green BAPTA-1 AM, by means of an air pressure pulse to brain tissue, resulting in a stained area with a diameter of 300–500 μm (Connor et al., 1999; Garaschuk et al., 2006; Stosiek et al., 2003). The method involves the trapping of AM calcium dye molecules into cells, neurons and glia (Kerr et al., 2005; Stosiek et al., 2003), owing to the removal of the hydrophobic ester residue by intracellular esterases (Tsien, 1981). In neurons, the somatic calcium signals are mediated by calcium entry through voltage-gated calcium channels due to action potential activity. In the absence of effective voltage imaging approaches in vivo, imaging of calcium as surrogate marker for the spiking activity is widely used for the analysis of local neuronal circuits in vitro and in vivo (Kerr et al., 2005; Mao et al., 2001; Ohki et al., 2005; Stosiek et al., 2003). An unambiguous identification of astrocytes can be achieved by either morphological analysis (astrocytes appear much brighter and their processes can be well distinguished) or coloading with the glial marker sulforhodamine 101 (Nimmerjahn et al., 2004). Moreover, AM loading is combinable with transgenic mouse lines or virally transduced animals that have fluorescent labeling of specific cell types, for example interneurons (Runyan et al., 2010; Sohya et al., 2007; Tamamaki et al., 2003). It is important to note that Hirase et al. (2004) developed a method that allows the exclusive labeling of astrocytes with fluorescent calcium indicators in vivo and the accurate analysis of glia-specific mechanisms of calcium signaling (Takano et al., 2006; Wang et al., 2006).

Besides AM calcium dyes, dextran-conjugated chemical calcium indicators can also be employed for network loading, mostly by pressure injection to axonal pathways where the dye molecules are taken up and transported antero- and retrogradely to the axon terminals and the cell bodies, respectively (Figure 3B, middle panel) (Gelperin and Flores, 1997). This approach is suitable for the labeling of populations of neurons and has been successfully used to record calcium signals from axonal terminals in the mouse cerebellum and olfactory bulb (Kreitzer et al., 2000; Oka et al., 2006; Wachowiak and Cohen, 2001) as well as calcium signals in spinal cord neurons (O'Donovan et al., 2005). Finally, electroporation is used not only for the labeling of single cells (see above), but also for the dye loading of local neuronal networks (Figure 3B, right panel) (Nagayama et al., 2007). This is achieved by inserting a micropipette containing the dye in salt-form or as dextran-conjugate into the brain or spinal cord area of interest and by applying trains of electrical current pulses. As a result, the dye is taken up by nearby cell bodies and cellular processes, presumably mostly the dendrites. This approach has been successfully utilized in vivo in mouse neocortex, olfactory bulb, and cerebellum (Nagayama et al., 2010, 2007). Variants of this method were used for calcium imaging recordings in whole-mounted adult mouse retina (Briggman and Euler, 2011) and in the antennal lobe of the silkmoth (Fujiwara et al., 2009).

In recent years, GECIs have become a widely used tool in neuroscience (Looger and Griesbeck, 2011). There are different possibilities of expressing GECIs in neurons, of which viral transduction is probably at present the most popular one (Figure 3C, left panel). The viral construct with the GECI can be targeted to specific brain areas by means of stereotaxic injection (Cetin et al., 2006). In principal, lenti- (LV) (Dittgen et al., 2004), adeno- (Soudais et al., 2004), adeno-associated (AAV) (Monahan and Samulski, 2000), herpes-simplex (Lilley et al., 2001), and recently ΔG rabies (Osakada et al., 2011) viral vectors are used to introduce GECIs into the cells of interest. One of the practically relevant differences between the various viral vectors is the size of the genome carried by the virus. For example, LV can contain up to 9 kb whereas AAV-based vectors are restricted to a size of only 4.7 kb (Dong et al., 1996; Kumar et al., 2001). At present, LV- and AAV-based vectors are probably most widely used (Zhang et al., 2007). Both vectors are characterized by a high "multiplicity-of-infection" (many copy numbers of the viral genome per cell) and thus provide high expression levels over long periods of time with only little reported adverse effects (Davidson and Breakefield, 2003). Importantly, there are multiple approaches how to obtain target specificity to specific cell types.

Besides viral tropisms for definite cell types (Nathanson et al., 2009b), specificity for defined cell populations can arise from the use of cell-type-specific promoters (Chhatwal et al., 2007; Nathanson et al., 2009a; Shevtsova et al., 2005) or from the combination of transgenic cell-type-specific Cre recombinase driver mouse and rat lines (Gong et al., 2007; Witten et al., 2011) with a recombinase-dependent viral vector (Wirth et al., 2007). The latter restricts the research to rat and mouse as animal models whereas the other approaches are applicable also in other species. Second, in utero electroporation of DNA plasmids encoding for the GECI can be used and results, in contrast to viral delivery, in a relatively sparser labeling (Figure 3C, middle panel) (Mank et al., 2008). Since the early reports several years ago (e.g., Tabata and Nakajima, 2001), in utero electroporation has emerged as an efficient method to deliver DNA into cerebral precursor cells and, as consequence, neurons (Shimogori and Ogawa, 2008). Similar to single-cell and bulk electroporation techniques (see above), in utero electroporation uses an electrical field to drive negatively charged DNA molecules into the cells (De Vry et al., 2010). The sizes of the transfected area as well as the neuronal specificity depend on the embryo's age and the electrode configuration (Borrell et al., 2005; Langevin et al., 2007). It is important to stress that in utero electroporation has the advantage that there are no limitations concerning the size of the transfected gene of interest and that it can be applied in species where transgenic technology is not easily implemented. Finally, generating transgenic mice expressing GECIs has been a challenge and initial attempts failed (Figure 3C, right panel) (Heim and Griesbeck, 2004; Nagai et al., 2004; Pologruto et al., 2004; Tsai et al., 2003). The precise reason for these failures is not entirely understood, but one problem seemed to be that a substantial fraction of the indicator protein was not functional when expressed in a transgenic mouse line (Hasan et al., 2004). Nevertheless, mice expressing GECIs would tremendously facilitate many experiments and a few transgenic lines are meanwhile available (Kotlikoff, 2007). For example, Hasan et al. (2004) reported the generation of two transgenic mouse lines expressing under a tetracycline-inducible promoter either camgaroo-2 or inverse pericam that was used for calcium imaging in the mouse olfactory bulb in vivo. Fletcher et al. (2009) show odor-evoked calcium responses in a transgenic mouse line expressing GCamp2 and finally Heim et al. (2007) report the presence of glutamate-induced calcium transients in the soma and dendrites of CerTN-L15-expressing neurons.

Chemical and genetically encoded calcium indicators have specific advantages and limitations that need to be taken into account when designing a new experiment. For example, chemical calcium indicators are characterized by a very good signal-to-noise ratio and rapid kinetics (e.g., Helmchen et al., 1997; Hendel et al., 2008). In addition, the methods for targeted dye loading to single cells or small groups of cells are well established (Figures 3A and 3B) and these methods are similar in various mammalian species. One limitation is that it is difficult to specifically label genetically defined classes of neurons—for example, a particular class of interneurons. Another serious limitation is the difficulty to perform chronic recordings over several days (Andermann et al., 2010). For such applications, GECIs are superior as they are functional in neurons over long time periods (Andermann et al., 2010; Mank et al., 2008; Tian et al., 2009). For chronic imaging over weeks and months they can be combined with the chronic window (Holtmaat et al., 2009) or thinned skull preparations (Yang et al., 2010). Unlike chemical indicators, GECIs allow, in conjunction with cell-type-specific promoters (Bozza et al., 2004), targeting sequences (Mao et al., 2008; Shigetomi et al., 2010), and the use of the Cre-loxP system (Luo et al., 2008), recordings from molecularly defined cell types or even subcellular compartments. Moreover, the FRET-based GECIs are rather insensitive to brain pulsation and motion artifacts, a feature that is particularly beneficial for measurements in awake, behaving animals (Lütcke et al., 2010). However, the delivery of GECIs through pipette-based viral transduction or through in utero electroporation can sometimes lead to heterogeneous cellular labeling and/or to tissue damage. Another not yet fully solved problem is the slow kinetics of most GECIs due to their rather slow on and off rates (e.g., Hendel et al., 2008). Furthermore, there is the potential problem of cytotoxicity, which is observed after long-term expression of various GECIs (e.g., GCaMP3, D3cpV, and TN-XXL) through in utero electroporation or viral transduction (Tian et al., 2009). In addition, expression of GECIs in transgenic animals may reduce their calcium sensing performance (Hasan et al., 2004). Currently, there are intense ongoing research efforts that lead to rapid improvements and a continuously growing range of applications of the various GECIs (Looger and Griesbeck, 2011; Zhao et al., 2011).

Common Calcium Imaging Devices

The main types of instrumentation that are used for calcium imaging are summarized in Figure 4. The light-sensing device is usually attached to a microscope and combined, depending on the specific application, with an appropriate light source for the excitation of the calcium indicator dyes. Figures 4A and 4B illustrate schematically two calcium imaging approaches involving wide-field microscopy (for review, see Homma et al., 2009). In these cases, the light source is usually a mercury or xenon lamp, allowing an easy change of the excitation wavelengths. Switching between two excitation wavelengths, as used in excitation ratiometric measurements, can be performed rapidly by using, for example, a filter wheel or a regulated monochromatic light source. Excitation and emission light is usually separated by a dichroic mirror that is located within the microscope. Calcium imaging can be performed by using photodiode arrays (Figure 4A) (Ross and Werman, 1987), devices that are not very common anymore, as well as by intensified video cameras (Smith and Augustine, 1988), by charged coupled detector (CCD)-based cameras (Figure 4B), and increasingly by complementary metal-oxide-semiconductor (CMOS)-based cameras (Baker et al., 2005; Carlson and Coulter, 2008). The classical photodiode arrays consist of a set of photodiodes (typically 124–1020 elements) (Grinvald et al., 1981). Each photodiode represents one pixel. Photodiode arrays are characterized by very high dynamic range and high speed but have a rather poor spatial resolution. CCD-based cameras consist of an array of photodiodes that are densely packed on a chip. In contrast to the traditional photodiode arrays, however, CCD-based cameras involve a serial read-out of the signals. Modern

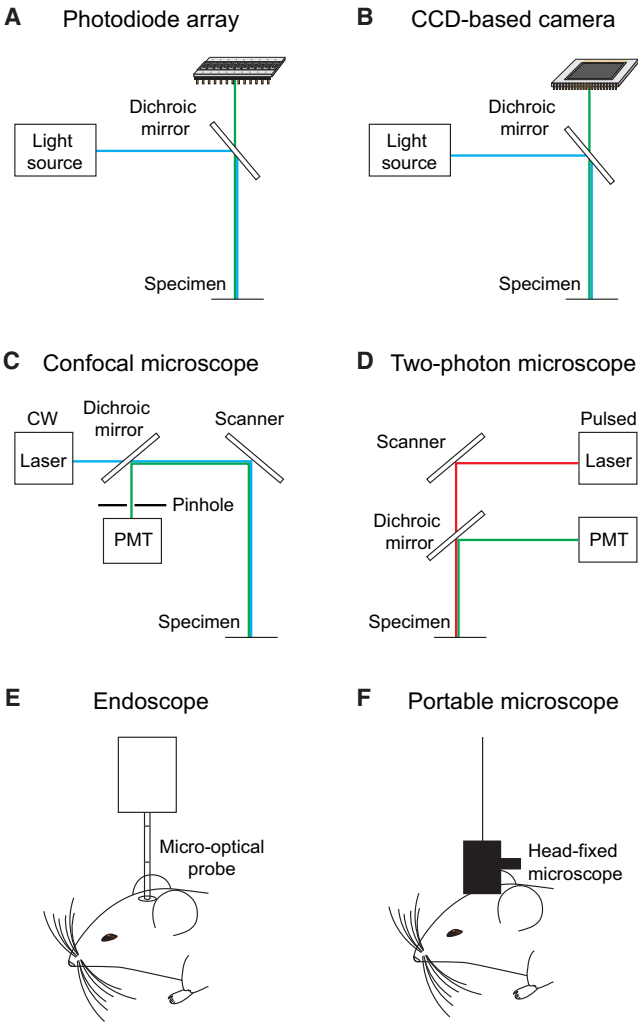

Figure 4. Common Imaging Devices

(A and B) Wide-field microcopy using a photodiode array (A) or a charged coupled device (CCD)-based (B) detection unit. In both cases the light source can be a mercury or xenon lamp. Excitation and emission light is separated by a dichroic mirror.

(C and D) Laser scanning microscopy. (C) Confocal microscopy using a continuous wave (CW) laser as light source. The excitation spot is steered across the specimen by a scanner. The emission light is descanned and reaches the photomultiplier tube (PMT) after passing a pinhole which is blocking out-of-focus fluorescence. Excitation and emission light is separated by a dichroic mirror. (D) Two-photon microscopy using a pulsed near-IR laser suitable for two-photon microscopy. The excitation spot is steered across the specimen by a scanner. The emitted fluorescence is detected by a photomultiplier tube (PMT).

(E and F) Imaging devices used for calcium imaging in non-head-fixed behaving animals. (E) Endoscopic approaches. (F) Portable head-mounted microscopes.

CCD-based cameras have an exquisitely high spatial and temporal resolution, but the noise level per pixel is high in some types of cameras. The contrast and resolution of wide-field microscopy based calcium imaging is limited by light scattering, especially when attempting to image neurons that are located deeper in the brain tissue (e.g., Denk and Svoboda, 1997). Therefore, these techniques are usually more appropriate for in vitro applications, like calcium imaging in neuronal cell cultures (Segal, 1995). In the in vivo situation, CCD-/CMOS-based cameras have found interesting applications in the imaging of large-scale calcium dynamics from the superficial cortical layers (e.g., Berger et al., 2007; Minderer et al., 2012).

Imaging calcium in neurons at deeper locations in the brain or spinal cord is usually performed by using confocal (Figure 4C) or two-photon microscopy (Figure 4D). Laser scanning microscopy generates the image by scanning a laser beam over the specimen (Lichtman and Conchello, 2005). The image is then created from the fluorescence values acquired for each pixel. Confocal microscopy usually involves one-photon excitation and, thus, the specimen is illuminated above and below the focal plane, which may cause photodamage in nonimaged regions. Figure 4C shows a schematic representation of a microscope design, in which optical sectioning is achieved by the implementation of a confocal aperture, a pinhole or slit, in an image-conjugated plane that blocks the out-of-focus fluorescence from reaching the detector unit (Conchello and Lichtman, 2005). Therefore, only photons that have been generated in the focal plane reach the photomultiplier tube (PMT). Unfortunately, the confocal aperture also blocks photons that are in fact generated in the focal plane, but are scattered on the way back through the optical pathway. This waste of photons becomes more and more critical when scattering increases when imaging deeper within the tissue. To compensate for the loss of ballistic photons due to scattering, excitation light power can be initially increased. This comes at the expense of increased tissue photodamage (in focus and out-of-focus), which can be high in confocal microscopy. Therefore, confocal microscopy, like wide-field microscopy, is mostly restricted to in vitro preparations, such as cultured neurons or brain slices. Finally, some applications benefit from the use of spinning disk-based confocal imaging involving the use of a rotating disk with a large number of fine pinholes, each of which acts each as an individual confocal aperture ("Nipkow disk") (Stephens and Allan, 2003; Takahara et al., 2011; Wilson, 2010). During imaging, many focal spots are illuminated simultaneously and the holes are arranged such that rotation of the disk causes the entire sample to be illuminated successively. A CCD-based camera can be used for image detection. Because of the simultaneous sampling from many focal points, this system can achieve higher image acquisition rates than laser scanning confocal microscopes.

The establishment of two-photon microscopy (Denk et al., 1990) that allows high-resolution and high-sensitivity fluorescence microscopy in highly scattering brain tissue in vivo was therefore an important step forward in the field of neuroscience (for review, see Svoboda and Yasuda, 2006) (Figure 4D). In two-photon microscopy, two low-energy near-IR photons cooperate to produce a transition from the ground to the excited state in a fluorescent molecule. This two-photon effect must occur within a femtosecond time window. Importantly, the process of two-photon absorption is nonlinear such that its rate depends on the second power of the light intensity. As a consequence, fluorophores are almost exclusively excited in a diffraction-limited focal volume ("localization of excitation") (Svoboda and Yasuda, 2006). Out-of-focus excitation and bleaching are strongly reduced. Only the development of pulsed

lasers suitable for two-photon microscopy, which are characterized by short pulses of about 100 fs duration containing a high photon density, allowed this process to be exploited for fluorescence microscopy in biological samples. Since excitation is bound to occur only in the focal spot, all fluorescence photons, ballistic or scattered, caught by the microscope and transmitted to the detecting photomultiplier (PMT) at a given time point can be used to generate the image (e.g., Denk et al., 1994). Another advantage is that the usual excitation wavelengths are within the near-IR spectrum, with a better tissue penetration than the visible light used in one-photon microscopy. This is due to the fact that these wavelengths are less scattered and less absorbed by natural chromophores present in the brain (e.g., Oheim et al., 2001). Importantly, the background fluorescence level is very low. For all those reasons, two-photon calcium imaging became the method of choice for recordings in deeper brain regions (for review, see Helmchen and Denk, 2005; Svoboda and Yasuda, 2006). Thus, cortical circuits can be examined in vivo with connections well preserved. Common two-photon lasers are tunable from 700 nm to 1000 nm or more and are suitable for the excitation of most commercially available fluorophores.

There are promising new approaches to extend the quality and versatility of two-photon microscopy and thereby two-photon calcium imaging. Inspired by imaging work that is performed in astronomy the use of adaptive optics in neurobiology aims at correcting in advance (before the illumination light is entering the optical pathway) for spherical aberrations that may distort the laser pulse and, therefore, may decrease the efficiency of two-photon imaging. These aberrations become increasingly more relevant with increasing depth (Girkin et al., 2009). The purpose of this correction is to obtain the optimal duration and shape of the laser pulse at the focal spot (Ji et al., 2010; Rueckel et al., 2006; Sherman et al., 2002). An interesting approach to increase depth penetration in two-photon microscopy is the use of regenerative laser amplifiers, which yields laser pulses with higher photon density, but at lower repetition rate. Because of the increased photon density, the probability for the two-photon effect is elevated, allowing, for example, the recording of sensory-evoked calcium signals from layer 5 pyramidal neuron somata in vivo (Mittmann et al., 2011). Present limitations of this technique are the lack of wavelength tunability and the decreased speed of imaging. Finally, the development of optical parametric oscillators (OPOs) pushes two-photon microscopy toward excitation wavelengths in the infrared spectrum (>1080 nm) and enables the efficient excitation of red-shifted fluorophores. As a result, it can increase imaging depth because of the reduced absorption and scattering at longer wavelengths (Andresen et al., 2009; Kobat et al., 2009). The speed of calcium imaging can be increased by the use of resonant galvo-scanners (Fan et al., 1999; Nguyen et al., 2001; Rochefort et al., 2009) or the use of acousto-optic deflectors (AOD) (Chen et al., 2011; Grewe et al., 2010; Iyer et al., 2006; Lechleiter et al., 2002; Otsu et al., 2008), especially when implementing the random-access imaging mode (Iyer et al., 2006; Kirkby et al., 2010; Otsu et al., 2008). Alternatively, multibeam confocal excitation also allows high imaging speed, but is restricted to superficial layers of nervous tissue and is so far only used in ex vivo preparations (Crépel et al., 2007). Next, there are increasing efforts for 3D imaging, involving various approaches (Cheng et al., 2011; Göbel and Helmchen, 2007; Göbel et al., 2007).

Even when using two-photon microscopy combined with improved depth penetration, imaging depth is ultimately limited (Andresen et al., 2009; Theer et al., 2003). A major limiting factor is the fluorescence generated by off-focus excitation light at the surface of the sample (Helmchen and Denk, 2005). Off-focus excitation increases necessarily because, in order to image deeper in the tissue, the laser intensity needs to be increased. This reduces dramatically the imaging quality. A not too elegant, but obvious approach for the recording from deeper brain regions is the mechanical removal of the covering tissue—for example the removal of cortical tissue located on top of the hippocampus (Dombeck et al., 2010; Mizrahi et al., 2004). Another way for the detection of calcium signals in deep brain structures involves microendoscopic approaches (Figure 4E). These include the insertion of optical fibers and fiber-like GRIN lenses alone or in conjunction with microprisms (Adelsberger et al., 2005; Chia and Levene, 2009; Flusberg et al., 2005; Grienberger et al., 2012; Jung et al., 2004; Levene et al., 2004; Murayama et al., 2007). GRIN-based microendoscopes, usually 350–1000 μm in diameter, comprise typically 1–3 gradient refractive index (GRIN) lenses that use internal variations in their refractive index to guide light to and back from the site of recording. Microendoscopes can, if coupled to an objective, project the scanning pattern into the focal plane, which lies inside the tissue and can also allow for changes in the axial position of the focal plane (Wilt et al., 2009). Their features, such as field-of-view size, numerical aperture, working distance, and physical length can be freely chosen. Complementary to these techniques, a dual-core microprobe that combines an optical core to locally excite and collect fluorescence with an electrolyte-filled core to record electrical signals has been developed (LeChasseur et al., 2011).

Finally, there are increasing efforts directed toward recordings in freely moving animals, involving the development of miniaturized head-mounted imaging devices (Engelbrecht et al., 2008; Flusberg et al., 2008; Helmchen et al., 2001; Sawinski et al., 2009). These imaging devices generally consist of two components (Figure 4F). A mobile component is fixed on the skull of the moving animal and contains the optical components. The other component is connected with the mobile one through an optical fiber and is usually immobile, containing the hard- and software for image recordings. The individual designs of these devices vary substantially. For example, whereas Helmchen et al. (2001) places nearly all components of a traditional microscope in the head-mounted mobile device (including objective, dichroic mirror, PMT, and scanner), Sawinski et al. (2009) included into the head-fixed component only the objective and the dichroic mirror. Recently, Ghosh et al. (2011) reported the development of a one photon-based and completely autochthone head-fixed camera-based device, usable for functional calcium measurements in freely moving animals.

Application Examples of Calcium Imaging

In the following we highlight several applications of calcium imaging obtained in mammalian neurons. It is needless to say that calcium imaging can be successfully performed in many

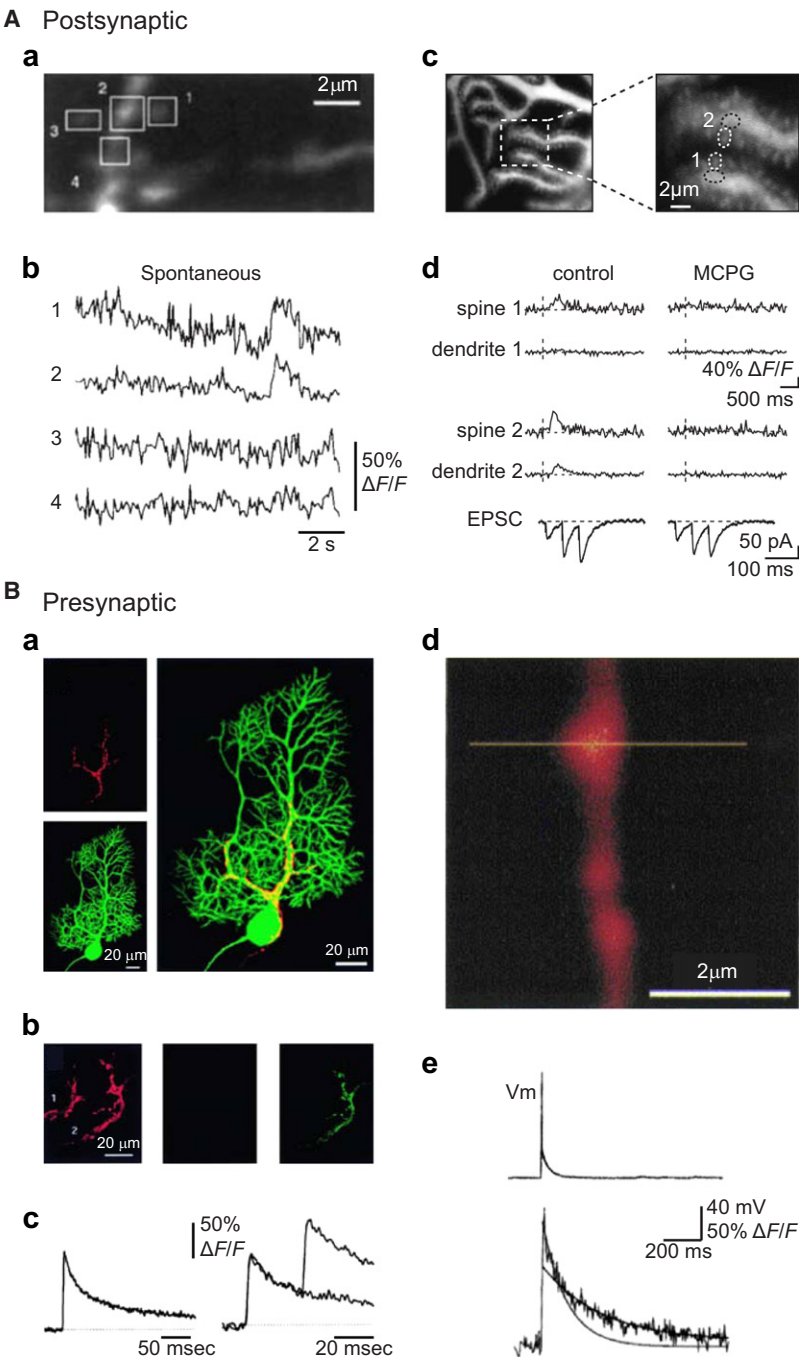

Figure 5. Calcium Imaging at the Synapse In Vitro

(A) Calcium imaging at the postsynaptic site. (Aa and Ab) Spine calcium signals recorded from a CA1 pyramidal neuron in a rat hippocampal slice preparation. (Aa) Image of a dendritic segment covered with many dendritic spines taken in a rat hippocampal slice. The CA1 pyramidal neuron was filled with Calcium Green-1 using the whole-cell patch-clamp configuration. The regions of interest (ROI) 1 and 3 contain dendritic spines whereas ROI 2 and ROI 4 are located on the dendritic shaft. (Ab) Calcium transients caused by spontaneous synaptic activity. Note that there are calcium transients only in ROI 1 and 2. Panels (Aa) and (Ab) adapted by permission from Yuste and Denk (1995). (Ac and Ad) Spine calcium signals recorded from a Purkinje cell in a cerebellar slice preparation. (Ac) Images of a Purkinje cell dendrite (left) with many dendritic spines (right). Dashed squares indicate ROIs (white dashed line: dendritic spine; black dashed line: dendritic shaft). (Ad) Fluorescence measurements taken from the ROIs shown in (Ac). In spine 1, the synaptic calcium transient was restricted to an individual spine. A large synaptic calcium transient was detected in spine 2 and a smaller signal occurred in the adjacent dendritic region. Note that MCPG (1mM), an antagonist of metabotropic glutamate receptors, completely blocked all observed calcium transients. The bottom traces illustrate the corresponding EPSCs evoked by a train of three stimuli (20 Hz). Panels (c) and (d) adapted by permission from Takechi et al. (1998).

(B) Calcium imaging at the presynaptic site. (Ba–Bc) Climbing fiber presynaptic terminals colabeled with the calcium indicator fluo-4 dextran and Texas red Dextran. (Ba) Confocal image stack of a Texas red dextran-labeled climbing fiber (left-upper panel) and the Purkinje cell onto which the climbing fiber synapses (left-lower panel). The Purkinje cell is labeled with the fluorescent marker Alexa Fluor 488. The overlay (right panel) shows the characteristic morphology of this synapse (the overlapping structures are shown in yellow). (Bb) Single section of a confocal image stack. Two climbing fibers are labeled with Texas red dextran (left). Image of these fibers at rest (middle) and during 20 Hz stimulation of fiber 2 (right) showing the fluo-4 channel. (Bc) Stimulus-evoked calcium transients for one (left) and two (right) stimuli. Panels (a)–(c) adapted with permission from Kreitzer et al. (2000). (Bd and Be) Calcium transients in a single bouton of a cortical layer 2/3 pyramidal neuron. (Bd) Presynaptic bouton of a cortical layer 2/3 pyramidal neuron loaded with Oregon Green BAPTA-1. Horizontal line indicates position of the line scan for the fluorescence measurements. (Be) The action potential evoked by somatic current injection is shown in the upper trace. Lower trace shows corresponding calcium transient recorded in the single bouton. Panels (d) and (e) adapted by permission from Koester and Sakmann (2000). Calcium signal amplitudes in all figures and throughout the text are given as the ratio of the relative fluorescence change and the baseline fluorescence (ΔF/F).

other species, including zebrafish (e.g., Brustein et al., 2003; Sumbre et al., 2008; Yaksi et al., 2009), *Aplysia* (e.g., Gitler and Spira, 1998), crayfish (e.g., Ravin et al., 1997), developing *Xenopus* (e.g., Demarque and Spitzer, 2010; Hiramoto and Cline, 2009; Tao et al., 2001), frog (e.g., Delaney et al., 2001), squid (e.g., Smith et al., 1993), turtle (e.g., Wachowiak et al., 2002), *Drosophila* (e.g., Seelig et al., 2010; Wang et al., 2003; Yu et al., 2003), blowfly (e.g., Elyada et al., 2009), and honey bee (e.g., Galizia et al., 1999).

Imaging Post- and Presynaptic Function In Vitro

Imaging dendritic spines, the postsynaptic site of excitatory connections in many neurons, was one of the first biological applications of two-photon calcium imaging. Combining two-photon microscopy with calcium imaging in hippocampal brain slices demonstrated that calcium signals can be restricted to dendritic spines (Figures 5Aa and 5Ab) (Yuste and Denk, 1995). The authors showed additionally that spine calcium signals were abolished by the application of the blockers of

glutamatergic transmission. Subsequently, synaptically evoked spine calcium signaling was found to be caused by a variety of other mechanisms, depending on the type of neuron (Denk et al., 1995; Finch and Augustine, 1998; Kovalchuk et al., 2000; Raymond and Redman, 2006; Wang et al., 2000). For example, Figures 5Ac and 5Ad show results obtained with confocal calcium imaging from mouse cerebellar parallel fiber-Purkinje cell synapses. The authors identified the calcium signaling mechanism of metabotropic glutamate receptor type 1-mediated transmission, involving calcium release from internal stores in dendrites and spines (Takechi et al., 1998). It has been shown that such a localized dendritic calcium signaling is essential for the induction of long-term synaptic depression (Konnerth et al., 1992; Wang et al., 2000), a possible cellular mechanism underlying motor learning in the cerebellum (Aiba et al., 1994; Bender et al., 2006).

Similarly, the calcium dynamics at presynaptic terminals are also accessible to calcium imaging (Delaney et al., 1989; Regehr and Tank, 1991a, 1991b; Rusakov et al., 2004; Smith et al., 1993). For this purpose, presynaptic terminals are loaded with an appropriate calcium indicator dye. A nice example is illustrated in Figures 5Ba–5Bc. To image climbing fibers in the cerebellar cortex, the authors injected the calcium indicator fluo-4 together with the morphological marker Texas red dextran upstream into the inferior olive of neonatal rats in vivo (Kreitzer et al., 2000). The dextran-conjugated calcium dye and Texas red were taken up by the inferior olive neurons and diffused within a few days through the climbing fibers to the cerebellar cortex. Thus, climbing fibers could be identified in subsequently prepared cerebellar slices. Purkinje cells were then counterlabeled with Alexa Fluor 488 (Figure 5Ba). This approach enabled the recording of stimulus-induced calcium signals in the presynaptic climbing fibers (Figures 5Bb and 5Bc). Another example involves calcium imaging of presynaptic boutons of cortical pyramidal neurons by Koester and Sakmann (2000), who combined two-photon microscopy and loading of the presynaptic terminals with Oregon Green BAPTA-1 via whole-cell recordings of the presynaptic neurons (Figure 5Bd and 5Be). Thus, they were able to record action-potential-evoked calcium signals in axonal boutons of cortical layer 2/3 pyramidal neurons of juvenile rats (Figure 5Be). These presynaptic calcium signals were found to be reliably inducible by only a single action potential. Interestingly, the large action-potential-evoked calcium signals were mostly localized to the boutons, but not the surrounding axonal segments.

Dendritic and Spine Calcium Signals In Vivo

In recent years, it has become possible to use two-photon microscopy for imaging dendritic and spine calcium signals in mammalian neurons in vivo (Chen et al., 2011; Helmchen et al., 1999; Jia et al., 2010; Svoboda et al., 1997; Svoboda et al., 1999; Takahashi et al., 2012; Waters and Helmchen, 2004). Svoboda et al. reported in 1997 for the first time dendritic calcium signals in vivo that were obtained from layer 2/3 rat pyramidal neurons (Figure 6A). They were able to record stimulus-associated dendritic calcium signals in barrel cortical neurons (Figures 6Ab–6Ad). The amplitude of these calcium signals was correlated to the number of action potentials and was largest in the proximal dendrite, suggesting that the signals were due to action

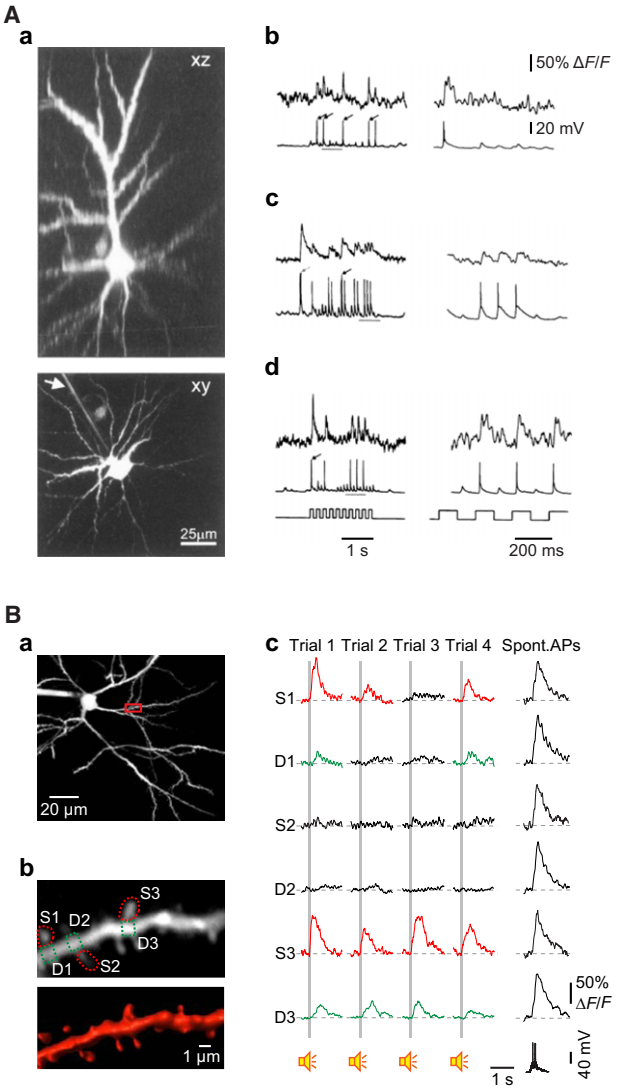

Figure 6. Dendritic and Spine Calcium Signals In Vivo

(A) Recording of dendritic calcium signals from a layer 2/3 pyramidal neuron of rat primary vibrissa cortex in vivo. (Aa) 3D reconstruction of a layer 2/3 pyramidal neuron labeled with calcium green-1. Upper panel: x-z projection. Lower panel: x-y projection. (Ab–Ad) Response of three representative cells to whisker stimulation. Left column: responses to an entire stimulus train (5 Hz, 2 s). Right column: expanded view showing only part of the entire stimulus period. Besides the recording of the membrane potential, recorded by a sharp microelectrode (lower trace), the dendritic calcium recording is shown (upper trace). The time course of the whisker stimulation is shown at the bottom. Recordings of dendritic calcium signals were performed at different positions in the apical dendrite for the three different cells. Adapted by permission from Svoboda et al. (1997).

(B) Recordings of spine calcium signals from a layer 2/3 pyramidal neuron of mouse primary auditory cortex in vivo. (Ba) Z-projection of a layer 2/3 neuron labeled with Oregon Green BAPTA-1. The red rectangle indicates the area magnified in (Bb). (Bb) Upper panel: image at high magnification of the dendritic segment indicated in (Ba). Three spines of interest (S1–S3) and the adjacent dendritic regions (D1–D3) are indicated by dashed lines. Lower panel: 3D image reconstruction of the dendritic segment. (Bc) Calcium transients evoked by auditory stimulation in spines (red) and corresponding dendritic shaft regions (green), as indicated in (Bb). Four consecutive trials of stimulation and a calcium transient evoked by backpropagation of action potentials (Spont. APs, spontaneous action potentials) are shown. Adapted by permission from Chen et al. (2011).

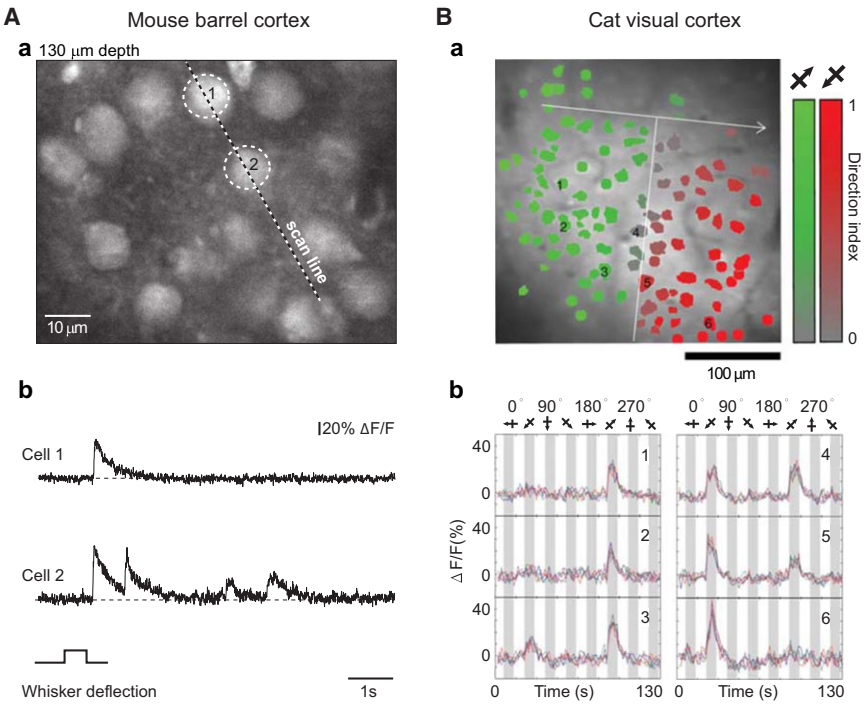

Figure 7. Circuit Analysis in Different Animal Models In Vivo

(A) In vivo recordings of calcium transients evoked by whisker deflection in mouse barrel cortex. (Aa) Image of layer 2/3 neurons in mouse barrel cortex in vivo. The calcium indicator Oregon Green BAPTA-1 AM was used for cell loading. (Ab) Line-scan recordings of calcium transients evoked in two neurons by a deflection of the majority of whiskers on the contralateral side of the mouse's snout. The position of the scanned line and the neurons analyzed are indicated in (a). Adapted by permission from Stosiek et al. (2003).

(B) In vivo recordings of calcium transients evoked by visual stimulation (drifting square-wave gratings of eight different directions separated each by 45°) in cat primary visual cortex. (Ba) Cell-based direction map; the color specifies the preferred direction for each cell according to its individual direction index (see color scale on right; green, 225°; red, 45°). The cells responding to both 45° and 225° are displayed as gray. The vertical white line below the arrow indicates approximate position of the direction discontinuity. (Bb) Single-trial time courses of six individual cells in response to drifting grating stimulation (indicated as 1–6 in Ba). Adapted by permission from Ohki et al. (2005).

potential back-propagation into the dendritic arbor. One role of these dendritic signals may be the amplification of calcium signals that are evoked by synaptic activity (Helmchen et al., 1999; Svoboda et al., 1997; Svoboda et al., 1999; Waters and Helmchen, 2004; Waters et al., 2003).

Besides the study of such backpropagation-evoked calcium signals, it became recently feasible to use calcium imaging for the investigation of the spatial and temporal distribution of synaptic inputs to cortical neurons in vivo (Chen et al., 2011; Jia et al., 2010; Varga et al., 2011). In these studies, the membrane potential of the neurons was slightly hyperpolarized to prevent action potential firing. Thus, it became possible to isolate local dendritic or even single spine calcium signals in response to sensory stimulation. The local calcium signals reflected specific sensory-evoked synaptic input sites on the dendrites of the respective neurons. Figure 6B shows, for example, the sensory-evoked calcium signals recorded by Chen et al. (2011) in the spines and dendrites of mouse layer 2/3 auditory cortex neurons (Figures 6Ba and 6Bb). The stable recording of such single spine calcium signals in vivo required the development of a new method named low-power temporal oversampling (LOTOS). LOTOS helps to increase the yield in fluorescence signal and to reduce phototoxic damage (Chen et al., 2011). The sound-evoked spine calcium signals were found to be, in agreement with previous in vitro studies (e.g., Yuste and Denk, 1995), mostly compartmentalized in dendritic spines (Figure 6Bc). Importantly, calcium imaging enabled the recording of many synaptic sites at the same time and, therefore, to map functionally the synaptic input sites of a specific neuron. While these studies relied on the use of chemical calcium indicators (Jia et al., 2011), we expect that in the future GECIs will be widely used to investigate dendritic calcium signals. A proof-of-principle study demonstrated already a few years ago that, using a transgenic mouse line expressing the Troponin-C-based calcium indicator CerTN-L15, it was possible to record glutamate-induced calcium signals from dendrites in vivo (Heim et al., 2007). Another approach for recording dendritic calcium signals in vivo involves the use of a so called "fiberoptic periscope" (Murayama and Larkum, 2009; Murayama et al., 2007). The periscope is composed of a GRIN lens and a micro-prism angled at 90°, which is inserted in the cortex. The method combines targeted AM loading of apical dendrites of cortical layer 5 pyramidal neurons with a chemical calcium indicator with horizontal fluorescence collection from the top cortical layers (Murayama et al., 2009). It uses one-photon excitation and, strictly speaking, it is not a conventional imaging method as it collects the average fluorescence from many layer 5 dendrites without generating an image. However, it is applicable in anesthetized as well as in awake behaving mice, and there are attempts to combine the periscope approach with two-photon imaging (Chia and Levene, 2009).

Circuit Analysis in Different Animal Models In Vivo

Combining two-photon microscopy with AM calcium dye loading allows the functional analysis of local cortical circuits (Greenberg et al., 2008; Ohki et al., 2005; Stosiek et al., 2003). This approach has been applied in many different animal models, including mouse, rat, cat, and ferret (Kerr et al., 2007; Li et al., 2008; Ohki et al., 2006; Rochefort et al., 2011). Figure 7A shows the first example of such an in vivo two-photon imaging experiment. The authors investigated the responsiveness of mouse barrel cortical neurons to whisker stimulation and demonstrated the feasibility of calcium imaging for the

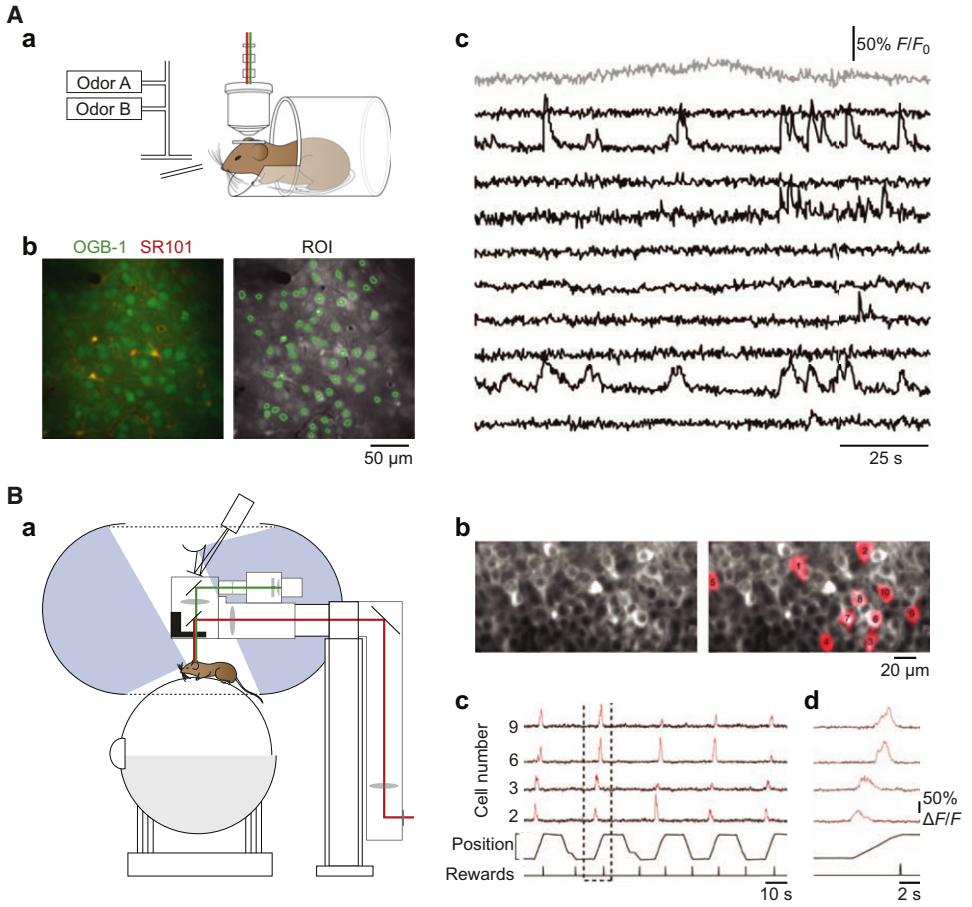

Figure 8. Calcium Imaging in the Behaving Animal

(A) Calcium imaging in the motor cortex of head-fixed mice engaged in an olfactory-related choice behavior with lick/no lick response. (Aa) Scheme of the experimental set-up showing a head-fixed mouse under a two-photon microscope while performing the task. The task consists of the differentiation between odor A and B. The mouse is trained to lick only in response to one of the two odors. (Ab) Two-photon image of layer 2/3 cells. Left, overlay of sulforhodamine 101 (SR101, red) and Oregon Green BAPTA-1 AM (green). Astrocytes are labeled by both dyes and thus appear yellow, whereas neurons are green. Right, regions of interest (ROI, green) overlaid on the Oregon Green BAPTA-1 channel. (Ac) Example of spontaneous calcium traces from ten neurons (black) and one astrocyte (gray). Panels (Ab) and (Ac) adapted by permission from Komiyama et al. (2010).

(B) Calcium imaging of place cells in the CA1 hippocampal region of mice which are placed on a spherical treadmill. (Ba) Experimental set-up: it consists of a spherical treadmill, a virtual reality apparatus (with projector and surrounding screens) and a custom-made two-photon microscope. (Bb) Two-photon images of neuron cell bodies in stratum pyramidale of CA1 labeled with the genetically encoded calcium indicator GCaMP3 (left). (Bc) Imaging CA1 place cells while the mouse is running along a virtual linear track. Calcium traces are shown in black. The respective regions of interest are shown in (Bb), right panel. Red traces indicate significant calcium transients. In parallel, the position of the mouse along the virtual linear track is recorded. Reward times are shown at the bottom. (Bd) Expanded view of the period indicated by the dashed box in (c). Panels (b)–(d) adapted by permission from Dombeck et al. (2010).

recording of action-potential-evoked activity with single-cell resolution (Stosiek et al., 2003). The AM loading approach has also been used in the cat to investigate the orientation preference of visual cortex neurons (Ohki et al., 2005) (Figure 7B). This study showed that orientation columns in the cat visual cortex are segregated with an extremely high spatial precision so that, even at the single cell level, areas of neurons with different orientation preference can be precisely distinguished. Examples of further studies using two-photon calcium imaging include recordings from mouse barrel (Sato et al., 2007), visual (Smith and Häusser, 2010), and auditory cortices (Bandyopadhyay et al., 2010; Rothschild et al., 2010) as well as from the mouse olfactory bulb (Wachowiak et al., 2004) and rat cerebellum (Sullivan et al., 2005). Various approaches can be used for extracting the action potential activity underlying such somatic calcium transients (Holekamp et al., 2008; Kerr et al., 2005; Sasaki et al., 2008; Vogelstein et al., 2010, 2009; Yaksi and Friedrich, 2006). For example, an effective approach is the "peeling algorithm" (Grewe et al., 2010), which is based on subtracting single action-potential-evoked calcium transients from the fluorescent trace until no additional event is present in the residual trace. Again, GECIs can be adapted as well for such studies of neuronal network function in different animal models (see also Table 1). Meanwhile, they have been used in rodents, *Drosophila*, *C. elegans*, zebrafish, and even primates (Díez-García et al., 2005; Heider et al., 2010; Higashijima et al., 2003; Horikawa et al., 2010; Li et al., 2005; Lütcke et al., 2010; Tian et al., 2009; Wallace et al., 2008; Wang et al., 2003).

A promising application of in vivo two-photon calcium imaging is the investigation of neuronal network plasticity. For example, experimental paradigms of visual deprivation (e.g., stripe rearing to influence orientation selectivity or unilateral eyelid closure to influence ocular dominance plasticity) have been shown to impact significantly the functional properties of mouse visual cortex neurons (Kreile et al., 2011; Mrsic-Flogel et al., 2007). Similarly, calcium imaging has been used to study the plasticity of neuronal networks in mouse models of disease, for example after ischemic damage of the somatosensory cortex (Winship and Murphy, 2008).

Calcium Imaging in Behaving Animals

There is a wide interest to examine brain circuits in relation to defined behaviors in awake animals. To achieve this, there are at present two major strategies involving calcium imaging as the central method for cellular functional analysis. One approach involves the use of head-mounted portable minimicroscopes (see section on imaging devices); the other concentrates on the study of head-fixed animals involving the use of standard two-photon microscopes. Figure 8A illustrates an experiment that was performed in the motor cortex of head-fixed mice that were engaged in an olfactory discrimination test (Komiyama et al., 2010). The animals were trained to lick in response to odor A and to stop licking in response to odor B (Figure 8Aa). The somatic calcium transients that were recorded in motor cortical neurons of the behaving mice had an excellent signal-to-noise ratio (Figures 8Ab–8Ac). Such experiments involving head fixation are possible because the mice have been gradually adapted to the experimental set-up, which includes the training in a tube-like construction which provides protection to the animal (in that particular study training lasted for 5 days on average). Another study examined the function of hippocampal neurons during a complex behavior. In this case, the mice were placed on a spherical treadmill on which they could run (Figure 8Ba) (Dombeck et al., 2009, 2007). The authors used two-photon calcium imaging of GCaMP3-labeled pyramidal neurons in the CA1 region of the hippocampus to study the spatial distribution of place cells (Figure 8Bb) (Dombeck et al., 2010). For this purpose, they removed a few days before the experiment some of the cortex tissue covering the hippocampus. In their experiments, they were able to map CA1 place cells by combining the positioning data from the spherical treadmill with the neuronal calcium signals (Figures 8Bb–8Bd). A remaining challenge of such studies is that it is very difficult to obtain calcium imaging and electrophysiological recordings from the same cell. Therefore, the relation between calcium transients and the underlying action potential activity is not yet entirely clear under these recording conditions. Furthermore, motion artifacts are often unavoidable, requiring the use of various motion correction algorithms (Dombeck et al., 2010, 2007; Komiyama et al., 2010). However, such experiments involving the use of GECIs can be repeated during consecutive days and weeks again and again, allowing an in-depth analysis of the mechanisms of neuronal plasticity in vivo (Andermann et al., 2010; Mank et al., 2008).

Outlook

What are the upcoming major challenges in neuronal calcium imaging? On the single-cell level, calcium imaging will remain an important tool for the analysis of the mechanisms associated with synaptic function and synaptic plasticity in specific types of neurons. The in vitro studies in combination with targeted mutations of neuronal signaling proteins can provide highly quantitative information on the intracellular mechanisms involving calcium signaling in specific neuronal subdomains, like spines and nerve terminals. The in vivo studies are likely to extend rapidly beyond the currently used layer 2/3 analysis, to neurons in deeper cortical layers, especially dendrites and somata in layer 4 and layer 5 of the mouse cortex. In combination with optogenetics, the combination of optics and genetics to achieve control over the activity of the target cells (Yizhar et al., 2011), such studies will contribute to a better understanding of local network function in the context of defined simple behaviors. Another important area that is likely to strongly expand in the coming years is calcium imaging in defined types of neurons in awake, behaving animals. These studies will not be restricted to mice and rats, but are likely to be increasingly extended also to other models, like ferrets, cats, and especially primates. An area of application with growing impact will be the use of calcium imaging in molecular medicine for a detailed analysis of signaling mechanisms in the explosively increasing number of disease models (Rochefort et al., 2008). We also expect further developments in calcium imaging technology, especially concerning devices capable of 3D imaging and miniaturized devices to be used in freely moving animals. Finally, calcium imaging may greatly benefit from the development of improved GECIs with higher signal sensitivity and better temporal response characteristics.

ACKNOWLEDGMENTS

We thank Jia Lou for excellent technical assistance. This work was supported by the Deutsche Forschungsgemeinschaft (IRTG 1373), the ERA-Net Program, the CIPSM cluster, and the Schiedel Foundation. A.K. is a Carl-von-Linde Senior Fellow of the Institute for Advanced Study of the TUM.

REFERENCES

Aaron, G., and Yuste, R. (2006). Reverse optical probing (ROPING) of neocortical circuits. Synapse *60*, 437–440.

Adelsberger, H., Garaschuk, O., and Konnerth, A. (2005). Cortical calcium waves in resting newborn mice. Nat. Neurosci. *8*, 988–990.

Aiba, A., Kano, M., Chen, C., Stanton, M.E., Fox, G.D., Herrup, K., Zwingman, T.A., and Tonegawa, S. (1994). Deficient cerebellar long-term depression and impaired motor learning in mGluR1 mutant mice. Cell *79*, 377–388.

Andermann, M.L., Kerlin, A.M., and Reid, R.C. (2010). Chronic cellular imaging of mouse visual cortex during operant behavior and passive viewing. Front Cell Neurosci *4*, 3.

Andresen, V., Alexander, S., Heupel, W.M., Hirschberg, M., Hoffman, R.M., and Friedl, P. (2009). Infrared multiphoton microscopy: subcellular-resolved deep tissue imaging. Curr. Opin. Biotechnol. *20*, 54–62.

Ashley, C.C., and Ridgway, E.B. (1968). Simultaneous recording of membrane potential, calcium transient and tension in single muscle fibers. Nature *219*, 1168–1169.

Badea, T., Goldberg, J., Mao, B., and Yuste, R. (2001). Calcium imaging of epileptiform events with single-cell resolution. J. Neurobiol. *48*, 215–227.

Baimbridge, K.G., Celio, M.R., and Rogers, J.H. (1992). Calcium-binding proteins in the nervous system. Trends Neurosci. *15*, 303–308.

Bakayan, A., Vaquero, C.F., Picazo, F., and Llopis, J. (2011). Red fluorescent protein-aequorin fusions as improved bioluminescent Ca^{2+} reporters in single cells and mice. PLoS ONE *6*, e19520.

Baker, B.J., Kosmidis, E.K., Vucinic, D., Falk, C.X., Cohen, L.B., Djurisic, M., and Zecevic, D. (2005). Imaging brain activity with voltage- and calcium-sensitive dyes. Cell. Mol. Neurobiol. *25*, 245–282.

Bandyopadhyay, S., Shamma, S.A., and Kanold, P.O. (2010). Dichotomy of functional organization in the mouse auditory cortex. Nat. Neurosci. *13*, 361–368.

Baubet, V., Le Mouellic, H., Campbell, A.K., Lucas-Meunier, E., Fossier, P., and Brúlet, P. (2000). Chimeric green fluorescent protein-aequorin as bioluminescent Ca^{2+} reporters at the single-cell level. Proc. Natl. Acad. Sci. USA *97*, 7260–7265.

Bender, V.A., Bender, K.J., Brasier, D.J., and Feldman, D.E. (2006). Two coincidence detectors for spike timing-dependent plasticity in somatosensory cortex. J. Neurosci. *26*, 4166–4177.

Berger, T., Borgdorff, A., Crochet, S., Neubauer, F.B., Lefort, S., Fauvet, B., Ferezou, I., Carleton, A., Lüscher, H.R., and Petersen, C.C. (2007). Combined voltage and calcium epifluorescence imaging in vitro and in vivo reveals subthreshold and suprathreshold dynamics of mouse barrel cortex. J. Neurophysiol. *97*, 3751–3762.

Berridge, M.J. (1993). Inositol trisphosphate and calcium signalling. Nature *361*, 315–325.

Berridge, M.J. (1998). Neuronal calcium signaling. Neuron *21*, 13–26.

Berridge, M.J., Bootman, M.D., and Roderick, H.L. (2003). Calcium signalling: dynamics, homeostasis and remodelling. Nat. Rev. Mol. Cell Biol. *4*, 517–529.

Berridge, M.J., Lipp, P., and Bootman, M.D. (2000). The versatility and universality of calcium signalling. Nat. Rev. Mol. Cell Biol. *1*, 11–21.

Bloodgood, B.L., and Sabatini, B.L. (2007a). $Ca^{(2+)}$ signaling in dendritic spines. Curr. Opin. Neurobiol. *17*, 345–351.

Bloodgood, B.L., and Sabatini, B.L. (2007b). Nonlinear regulation of unitary synaptic signals by $Ca_V(2.3)$ voltage-sensitive calcium channels located in dendritic spines. Neuron *53*, 249–260.

Bonifazi, P., Goldin, M., Picardo, M.A., Jorquera, I., Cattani, A., Bianconi, G., Represa, A., Ben-Ari, Y., and Cossart, R. (2009). GABAergic hub neurons orchestrate synchrony in developing hippocampal networks. Science *326*, 1419–1424.

Borrell, V., Yoshimura, Y., and Callaway, E.M. (2005). Targeted gene delivery to telencephalic inhibitory neurons by directional in utero electroporation. J. Neurosci. Methods *143*, 151–158.

Bowie, D., and Mayer, M.L. (1995). Inward rectification of both AMPA and kainate subtype glutamate receptors generated by polyamine-mediated ion channel block. Neuron *15*, 453–462.

Bozza, T., McGann, J.P., Mombaerts, P., and Wachowiak, M. (2004). In vivo imaging of neuronal activity by targeted expression of a genetically encoded probe in the mouse. Neuron *42*, 9–21.

Briggman, K.L., and Euler, T. (2011). Bulk electroporation and population calcium imaging in the adult mammalian retina. J. Neurophysiol. *105*, 2601–2609.

Brini, M. (2008). Calcium-sensitive photoproteins. Methods *46*, 160–166.

Brown, J.E., Cohen, L.B., De Weer, P., Pinto, L.H., Ross, W.N., and Salzberg, B.M. (1975). Rapid changes in intracellular free calcium concentration. Detection by metallochromic indicator dyes in squid giant axon. Biophys. J. *15*, 1155–1160.

Brustein, E., Marandi, N., Kovalchuk, Y., Drapeau, P., and Konnerth, A. (2003). "In vivo" monitoring of neuronal network activity in zebrafish by two-photon $Ca^{(2+)}$ imaging. Pflugers Arch. *446*, 766–773.

Burnashev, N., Zhou, Z., Neher, E., and Sakmann, B. (1995). Fractional calcium currents through recombinant GluR channels of the NMDA, AMPA and kainate receptor subtypes. J. Physiol. *485*, 403–418.

Carlson, G.C., and Coulter, D.A. (2008). In vitro functional imaging in brain slices using fast voltage-sensitive dye imaging combined with whole-cell patch recording. Nat. Protoc. *3*, 249–255.

Catterall, W.A. (2000). Structure and regulation of voltage-gated Ca^{2+} channels. Annu. Rev. Cell Dev. Biol. *16*, 521–555.

Cetin, A., Komai, S., Eliava, M., Seeburg, P.H., and Osten, P. (2006). Stereotaxic gene delivery in the rodent brain. Nat. Protoc. *1*, 3166–3173.

Chalasani, S.H., Chronis, N., Tsunozaki, M., Gray, J.M., Ramot, D., Goodman, M.B., and Bargmann, C.I. (2007). Dissecting a circuit for olfactory behaviour in Caenorhabditis elegans. Nature *450*, 63–70.

Chen, X., Kovalchuk, Y., Adelsberger, H., Henning, H.A., Sausbier, M., Wietzorrek, G., Ruth, P., Yarom, Y., and Konnerth, A. (2010). Disruption of the olivo-cerebellar circuit by Purkinje neuron-specific ablation of BK channels. Proc. Natl. Acad. Sci. USA *107*, 12323–12328.

Chen, X., Leischner, U., Rochefort, N.L., Nelken, I., and Konnerth, A. (2011). Functional mapping of single spines in cortical neurons in vivo. Nature *475*, 501–505.

Cheng, A., Gonçalves, J.T., Golshani, P., Arisaka, K., and Portera-Cailliau, C. (2011). Simultaneous two-photon calcium imaging at different depths with spatiotemporal multiplexing. Nat. Methods *8*, 139–142.

Chhatwal, J.P., Hammack, S.E., Jasnow, A.M., Rainnie, D.G., and Ressler, K.J. (2007). Identification of cell-type-specific promoters within the brain using lentiviral vectors. Gene Ther. *14*, 575–583.

Chia, T.H., and Levene, M.J. (2009). Microprisms for in vivo multilayer cortical imaging. J. Neurophysiol. *102*, 1310–1314.

Chiesa, A., Rapizzi, E., Tosello, V., Pinton, P., de Virgilio, M., Fogarty, K.E., and Rizzuto, R. (2001). Recombinant aequorin and green fluorescent protein as valuable tools in the study of cell signalling. Biochem. J. *355*, 1–12.

Clem, R.L., and Barth, A. (2006). Pathway-specific trafficking of native AMPARs by in vivo experience. Neuron *49*, 663–670.

Cobbold, P.H., and Rink, T.J. (1987). Fluorescence and bioluminescence measurement of cytoplasmic free calcium. Biochem. J. *248*, 313–328.

Conchello, J.A., and Lichtman, J.W. (2005). Optical sectioning microscopy. Nat. Methods *2*, 920–931.

Connor, J.A. (1986). Digital imaging of free calcium changes and of spatial gradients in growing processes in single, mammalian central nervous system cells. Proc. Natl. Acad. Sci. USA *83*, 6179–6183.

Connor, J.A., Razani-Boroujerdi, S., Greenwood, A.C., Cormier, R.J., Petrozzino, J.J., and Lin, R.C. (1999). Reduced voltage-dependent Ca^{2+} signaling in CA1 neurons after brief ischemia in gerbils. J. Neurophysiol. *81*, 299–306.

Coulter, D.A., Huguenard, J.R., and Prince, D.A. (1989). Calcium currents in rat thalamocortical relay neurones: kinetic properties of the transient, low-threshold current. J. Physiol. *414*, 587–604.

Crépel, V., Aronov, D., Jorquera, I., Represa, A., Ben-Ari, Y., and Cossart, R. (2007). A parturition-associated nonsynaptic coherent activity pattern in the developing hippocampus. Neuron *54*, 105–120.

Davidson, B.L., and Breakefield, X.O. (2003). Viral vectors for gene delivery to the nervous system. Nat. Rev. Neurosci. *4*, 353–364.

De Vry, J., Martínez-Martínez, P., Losen, M., Temel, Y., Steckler, T., Steinbusch, H.W., De Baets, M.H., and Prickaerts, J. (2010). In vivo electroporation of the central nervous system: a non-viral approach for targeted gene delivery. Prog. Neurobiol. *92*, 227–244.

Delaney, K., Davison, I., and Denk, W. (2001). Odour-evoked $[Ca^{2+}]$ transients in mitral cell dendrites of frog olfactory glomeruli. Eur. J. Neurosci. *13*, 1658–1672.

Delaney, K.R., Zucker, R.S., and Tank, D.W. (1989). Calcium in motor nerve terminals associated with posttetanic potentiation. J. Neurosci. *9*, 3558–3567.

Demarque, M., and Spitzer, N.C. (2010). Activity-dependent expression of Lmx1b regulates specification of serotonergic neurons modulating swimming behavior. Neuron *67*, 321–334.

Denk, W., Delaney, K.R., Gelperin, A., Kleinfeld, D., Strowbridge, B.W., Tank, D.W., and Yuste, R. (1994). Anatomical and functional imaging of neurons using 2-photon laser scanning microscopy. J. Neurosci. Methods *54*, 151–162.

Denk, W., Strickler, J.H., and Webb, W.W. (1990). Two-photon laser scanning fluorescence microscopy. Science *248*, 73–76.

Denk, W., Sugimori, M., and Llinás, R. (1995). Two types of calcium response limited to single spines in cerebellar Purkinje cells. Proc. Natl. Acad. Sci. USA *92*, 8279–8282.

Denk, W., and Svoboda, K. (1997). Photon upmanship: why multiphoton imaging is more than a gimmick. Neuron *18*, 351–357.

Díez-García, J., Matsushita, S., Mutoh, H., Nakai, J., Ohkura, M., Yokoyama, J., Dimitrov, D., and Knöpfel, T. (2005). Activation of cerebellar parallel fibers monitored in transgenic mice expressing a fluorescent Ca^{2+} indicator protein. Eur. J. Neurosci. *22*, 627–635.

Dittgen, T., Nimmerjahn, A., Komai, S., Licznerski, P., Waters, J., Margrie, T.W., Helmchen, F., Denk, W., Brecht, M., and Osten, P. (2004). Lentivirus-based genetic manipulations of cortical neurons and their optical and electrophysiological monitoring in vivo. Proc. Natl. Acad. Sci. USA *101*, 18206–18211.

Dombeck, D.A., Graziano, M.S., and Tank, D.W. (2009). Functional clustering of neurons in motor cortex determined by cellular resolution imaging in awake behaving mice. J. Neurosci. *29*, 13751–13760.

Dombeck, D.A., Harvey, C.D., Tian, L., Looger, L.L., and Tank, D.W. (2010). Functional imaging of hippocampal place cells at cellular resolution during virtual navigation. Nat. Neurosci. *13*, 1433–1440.

Dombeck, D.A., Khabbaz, A.N., Collman, F., Adelman, T.L., and Tank, D.W. (2007). Imaging large-scale neural activity with cellular resolution in awake, mobile mice. Neuron *56*, 43–57.

Dong, J.Y., Fan, P.D., and Frizzell, R.A. (1996). Quantitative analysis of the packaging capacity of recombinant adeno-associated virus. Hum. Gene Ther. *7*, 2101–2112.

Duchen, M.R. (1999). Contributions of mitochondria to animal physiology: from homeostatic sensor to calcium signalling and cell death. J. Physiol. *516*, 1–17.

Dulhunty, A.F. (2006). Excitation-contraction coupling from the 1950s into the new millennium. Clin. Exp. Pharmacol. Physiol. *33*, 763–772.

Eilers, J., Augustine, G.J., and Konnerth, A. (1995). Subthreshold synaptic Ca^{2+} signalling in fine dendrites and spines of cerebellar Purkinje neurons. Nature *373*, 155–158.

Eilers, J., and Konnerth, A. (2009). Dye loading with patch pipettes. Cold Spring Harb Protoc *2009*, pdb.prot5201.

Elyada, Y.M., Haag, J., and Borst, A. (2009). Different receptive fields in axons and dendrites underlie robust coding in motion-sensitive neurons. Nat. Neurosci. *12*, 327–332.

Engelbrecht, C.J., Johnston, R.S., Seibel, E.J., and Helmchen, F. (2008). Ultra-compact fiber-optic two-photon microscope for functional fluorescence imaging in vivo. Opt. Express *16*, 5556–5564.

Fan, G.Y., Fujisaki, H., Miyawaki, A., Tsay, R.K., Tsien, R.Y., and Ellisman, M.H. (1999). Video-rate scanning two-photon excitation fluorescence microscopy and ratio imaging with cameleons. Biophys. J. *76*, 2412–2420.

Feller, M.B., Wellis, D.P., Stellwagen, D., Werblin, F.S., and Shatz, C.J. (1996). Requirement for cholinergic synaptic transmission in the propagation of spontaneous retinal waves. Science *272*, 1182–1187.

Ferraguti, F., and Shigemoto, R. (2006). Metabotropic glutamate receptors. Cell Tissue Res. *326*, 483–504.

Finch, E.A., and Augustine, G.J. (1998). Local calcium signalling by inositol-1,4,5-trisphosphate in Purkinje cell dendrites. Nature *396*, 753–756.

Fletcher, M.L., Masurkar, A.V., Xing, J., Imamura, F., Xiong, W., Nagayama, S., Mutoh, H., Greer, C.A., Knöpfel, T., and Chen, W.R. (2009). Optical imaging of postsynaptic odor representation in the glomerular layer of the mouse olfactory bulb. J. Neurophysiol. *102*, 817–830.

Flusberg, B.A., Cocker, E.D., Piyawattanametha, W., Jung, J.C., Cheung, E.L., and Schnitzer, M.J. (2005). Fiber-optic fluorescence imaging. Nat. Methods *2*, 941–950.

Flusberg, B.A., Nimmerjahn, A., Cocker, E.D., Mukamel, E.A., Barretto, R.P., Ko, T.H., Burns, L.D., Jung, J.C., and Schnitzer, M.J. (2008). High-speed, miniaturized fluorescence microscopy in freely moving mice. Nat. Methods *5*, 935–938.

Fucile, S. (2004). Ca^{2+} permeability of nicotinic acetylcholine receptors. Cell Calcium *35*, 1–8.

Fujiwara, T., Kazawa, T., Haupt, S.S., and Kanzaki, R. (2009). Ca^{2+} imaging of identifiable neurons labeled by electroporation in insect brains. Neuroreport *20*, 1061–1065.

Galizia, C.G., Sachse, S., Rappert, A., and Menzel, R. (1999). The glomerular code for odor representation is species specific in the honeybee Apis mellifera. Nat. Neurosci. *2*, 473–478.

Garaschuk, O., Hanse, E., and Konnerth, A. (1998). Developmental profile and synaptic origin of early network oscillations in the CA1 region of rat neonatal hippocampus. J. Physiol. *507*, 219–236.

Garaschuk, O., Linn, J., Eilers, J., and Konnerth, A. (2000). Large-scale oscillatory calcium waves in the immature cortex. Nat. Neurosci. *3*, 452–459.

Garaschuk, O., Milos, R.I., and Konnerth, A. (2006). Targeted bulk-loading of fluorescent indicators for two-photon brain imaging in vivo. Nat. Protoc. *1*, 380–386.

Garaschuk, O., Schneggenburger, R., Schirra, C., Tempia, F., and Konnerth, A. (1996). Fractional Ca^{2+} currents through somatic and dendritic glutamate receptor channels of rat hippocampal CA1 pyramidal neurones. J. Physiol. *491*, 757–772.

Geiger, J.R., Melcher, T., Koh, D.S., Sakmann, B., Seeburg, P.H., Jonas, P., and Monyer, H. (1995). Relative abundance of subunit mRNAs determines gating and Ca^{2+} permeability of AMPA receptors in principal neurons and interneurons in rat CNS. Neuron *15*, 193–204.

Gelperin, A., and Flores, J. (1997). Vital staining from dye-coated microprobes identifies new olfactory interneurons for optical and electrical recording. J. Neurosci. Methods *72*, 97–108.

Ghosh, K.K., Burns, L.D., Cocker, E.D., Nimmerjahn, A., Ziv, Y., Gamal, A.E., and Schnitzer, M.J. (2011). Miniaturized integration of a fluorescence microscope. Nat. Methods *8*, 871–878.

Girkin, J.M., Poland, S., and Wright, A.J. (2009). Adaptive optics for deeper imaging of biological samples. Curr. Opin. Biotechnol. *20*, 106–110.

Gitler, D., and Spira, M.E. (1998). Real time imaging of calcium-induced localized proteolytic activity after axotomy and its relation to growth cone formation. Neuron *20*, 1123–1135.

Göbel, W., and Helmchen, F. (2007). New angles on neuronal dendrites in vivo. J. Neurophysiol. *98*, 3770–3779.

Göbel, W., Kampa, B.M., and Helmchen, F. (2007). Imaging cellular network dynamics in three dimensions using fast 3D laser scanning. Nat. Methods *4*, 73–79.

Goldberg, J.H., Tamas, G., Aronov, D., and Yuste, R. (2003). Calcium microdomains in aspiny dendrites. Neuron *40*, 807–821.

Gong, S., Doughty, M., Harbaugh, C.R., Cummins, A., Hatten, M.E., Heintz, N., and Gerfen, C.R. (2007). Targeting Cre recombinase to specific neuron populations with bacterial artificial chromosome constructs. J. Neurosci. *27*, 9817–9823.

Greenberg, D.S., Houweling, A.R., and Kerr, J.N. (2008). Population imaging of ongoing neuronal activity in the visual cortex of awake rats. Nat. Neurosci. *11*, 749–751.

Grewe, B.F., Langer, D., Kasper, H., Kampa, B.M., and Helmchen, F. (2010). High-speed in vivo calcium imaging reveals neuronal network activity with near-millisecond precision. Nat. Methods *7*, 399–405.

Grienberger, C., Adelsberger, H., Stroh, A., Milos, R.I., Garaschuk, O., Schierloh, A., Nelken, I., and Konnerth, A. (2012). Sound-evoked network calcium transients in mouse auditory cortex in vivo. J. Physiol. *590*, 899–918.

Grinvald, A., Cohen, L.B., Lesher, S., and Boyle, M.B. (1981). Simultaneous optical monitoring of activity of many neurons in invertebrate ganglia using a 124-element photodiode array. J. Neurophysiol. *45*, 829–840.

Grynkiewicz, G., Poenie, M., and Tsien, R.Y. (1985). A new generation of Ca^{2+} indicators with greatly improved fluorescence properties. J. Biol. Chem. *260*, 3440–3450.

Hallett, M., and Carbone, E. (1972). Studies of calcium influx into squid giant axons with aequorin. J. Cell. Physiol. *80*, 219–226.

Hartmann, J., Dragicevic, E., Adelsberger, H., Henning, H.A., Sumser, M., Abramowitz, J., Blum, R., Dietrich, A., Freichel, M., Flockerzi, V., et al. (2008). TRPC3 channels are required for synaptic transmission and motor coordination. Neuron *59*, 392–398.

Hasan, M.T., Friedrich, R.W., Euler, T., Larkum, M.E., Giese, G., Both, M., Duebel, J., Waters, J., Bujard, H., Griesbeck, O., et al. (2004). Functional fluorescent Ca^{2+} indicator proteins in transgenic mice under TET control. PLoS Biol. *2*, e163.

Head, J.F., Inouye, S., Teranishi, K., and Shimomura, O. (2000). The crystal structure of the photoprotein aequorin at 2.3 A resolution. Nature *405*, 372–376.

Heider, B., Nathanson, J.L., Isacoff, E.Y., Callaway, E.M., and Siegel, R.M. (2010). Two-photon imaging of calcium in virally transfected striate cortical neurons of behaving monkey. PLoS ONE *5*, e13829.

Heim, N., Garaschuk, O., Friedrich, M.W., Mank, M., Milos, R.I., Kovalchuk, Y., Konnerth, A., and Griesbeck, O. (2007). Improved calcium imaging in transgenic mice expressing a troponin C-based biosensor. Nat. Methods *4*, 127–129.

Heim, N., and Griesbeck, O. (2004). Genetically encoded indicators of cellular calcium dynamics based on troponin C and green fluorescent protein. J. Biol. Chem. *279*, 14280–14286.

Helmchen, F., Borst, J.G., and Sakmann, B. (1997). Calcium dynamics associated with a single action potential in a CNS presynaptic terminal. Biophys. J. *72*, 1458–1471.

Helmchen, F., and Denk, W. (2005). Deep tissue two-photon microscopy. Nat. Methods *2*, 932–940.

Helmchen, F., Fee, M.S., Tank, D.W., and Denk, W. (2001). A miniature head-mounted two-photon microscope. high-resolution brain imaging in freely moving animals. Neuron *31*, 903–912.

Helmchen, F., Imoto, K., and Sakmann, B. (1996). Ca^{2+} buffering and action potential-evoked Ca^{2+} signaling in dendrites of pyramidal neurons. Biophys. J. *70*, 1069–1081.

Helmchen, F., and Konnerth, A. (2011). Imaging in neuroscience: a laboratory manual (Cold Spring Harbor, N.Y: Cold Spring Harbor Laboratory Press).

Helmchen, F., Svoboda, K., Denk, W., and Tank, D.W. (1999). In vivo dendritic calcium dynamics in deep-layer cortical pyramidal neurons. Nat. Neurosci. *2*, 989–996.

Helmchen, F., and Waters, J. (2002). Ca^{2+} imaging in the mammalian brain in vivo. Eur. J. Pharmacol. *447*, 119–129.

Hendel, T., Mank, M., Schnell, B., Griesbeck, O., Borst, A., and Reiff, D.F. (2008). Fluorescence changes of genetic calcium indicators and OGB-1 correlated with neural activity and calcium in vivo and in vitro. J. Neurosci. *28*, 7399–7411.

Higashijima, S., Masino, M.A., Mandel, G., and Fetcho, J.R. (2003). Imaging neuronal activity during zebrafish behavior with a genetically encoded calcium indicator. J. Neurophysiol. *90*, 3986–3997.

Higley, M.J., and Sabatini, B.L. (2008). Calcium signaling in dendrites and spines: practical and functional considerations. Neuron *59*, 902–913.

Hiramoto, M., and Cline, H.T. (2009). Convergence of multisensory inputs in Xenopus tadpole tectum. Dev. Neurobiol. *69*, 959–971.

Hirase, H., Qian, L., Barthó, P., and Buzsáki, G. (2004). Calcium dynamics of cortical astrocytic networks in vivo. PLoS Biol. *2*, E96.

Holekamp, T.F., Turaga, D., and Holy, T.E. (2008). Fast three-dimensional fluorescence imaging of activity in neural populations by objective-coupled planar illumination microscopy. Neuron *57*, 661–672.

Holtmaat, A., Bonhoeffer, T., Chow, D.K., Chuckowree, J., De Paola, V., Hofer, S.B., Hübener, M., Keck, T., Knott, G., Lee, W.C., et al. (2009). Long-term, high-resolution imaging in the mouse neocortex through a chronic cranial window. Nat. Protoc. *4*, 1128–1144.

Homma, R., Baker, B.J., Jin, L., Garaschuk, O., Konnerth, A., Cohen, L.B., and Zecevic, D. (2009). Wide-field and two-photon imaging of brain activity with voltage- and calcium-sensitive dyes. Philos. Trans. R. Soc. Lond. B Biol. Sci. *364*, 2453–2467.

Hoogland, T.M., and Saggau, P. (2004). Facilitation of L-type Ca^{2+} channels in dendritic spines by activation of β_2 adrenergic receptors. J. Neurosci. *24*, 8416–8427.

Horikawa, K., Yamada, Y., Matsuda, T., Kobayashi, K., Hashimoto, M., Matsuura, T., Miyawaki, A., Michikawa, T., Mikoshiba, K., and Nagai, T. (2010). Spontaneous network activity visualized by ultrasensitive $Ca^{(2+)}$ indicators, yellow Cameleon-Nano. Nat. Methods *7*, 729–732.

Inouye, S., Noguchi, M., Sakaki, Y., Takagi, Y., Miyata, T., Iwanaga, S., Miyata, T., and Tsuji, F.I. (1985). Cloning and sequence analysis of cDNA for the luminescent protein aequorin. Proc. Natl. Acad. Sci. USA *82*, 3154–3158.

Iyer, V., Hoogland, T.M., and Saggau, P. (2006). Fast functional imaging of single neurons using random-access multiphoton (RAMP) microscopy. J. Neurophysiol. *95*, 535–545.

Jaffe, D.B., Johnston, D., Lasser-Ross, N., Lisman, J.E., Miyakawa, H., and Ross, W.N. (1992). The spread of Na^{+} spikes determines the pattern of dendritic Ca^{2+} entry into hippocampal neurons. Nature *357*, 244–246.

Jares-Erijman, E.A., and Jovin, T.M. (2003). FRET imaging. Nat. Biotechnol. *21*, 1387–1395.

Ji, N., Milkie, D.E., and Betzig, E. (2010). Adaptive optics via pupil segmentation for high-resolution imaging in biological tissues. Nat. Methods *7*, 141–147.

Jia, H., Rochefort, N.L., Chen, X., and Konnerth, A. (2010). Dendritic organization of sensory input to cortical neurons in vivo. Nature *464*, 1307–1312.

Jia, H., Rochefort, N.L., Chen, X., and Konnerth, A. (2011). In vivo two-photon imaging of sensory-evoked dendritic calcium signals in cortical neurons. Nat. Protoc. *6*, 28–35.

Johnson, I.D., and Spence, M.T.Z. (2010). Molecular Probes Handbook, A guide to fluorescecent probes and labeling technologies, 11th Edition (Eugene, OR, USA: Molecular Probes).

Jonas, P., Racca, C., Sakmann, B., Seeburg, P.H., and Monyer, H. (1994). Differences in Ca^{2+} permeability of AMPA-type glutamate receptor channels in neocortical neurons caused by differential GluR-B subunit expression. Neuron *12*, 1281–1289.

Judkewitz, B., Rizzi, M., Kitamura, K., and Häusser, M. (2009). Targeted single-cell electroporation of mammalian neurons in vivo. Nat. Protoc. *4*, 862–869.

Jung, J.C., Mehta, A.D., Aksay, E., Stepnoski, R., and Schnitzer, M.J. (2004). In vivo mammalian brain imaging using one- and two-photon fluorescence microendoscopy. J. Neurophysiol. *92*, 3121–3133.

Kano, M., Garaschuk, O., Verkhratsky, A., and Konnerth, A. (1995). Ryanodine receptor-mediated intracellular calcium release in rat cerebellar Purkinje neurones. J. Physiol. *487*, 1–16.

Kerr, J.N., de Kock, C.P., Greenberg, D.S., Bruno, R.M., Sakmann, B., and Helmchen, F. (2007). Spatial organization of neuronal population responses in layer 2/3 of rat barrel cortex. J. Neurosci. *27*, 13316–13328.

Kerr, J.N., Greenberg, D., and Helmchen, F. (2005). Imaging input and output of neocortical networks in vivo. Proc. Natl. Acad. Sci. USA *102*, 14063–14068.

Kirkby, P.A., Srinivas Nadella, K.M., and Silver, R.A. (2010). A compact Acousto-Optic Lens for 2D and 3D femtosecond based 2-photon microscopy. Opt. Express *18*, 13721–13745.

Kitamura, K., Judkewitz, B., Kano, M., Denk, W., and Häusser, M. (2008). Targeted patch-clamp recordings and single-cell electroporation of unlabeled neurons in vivo. Nat. Methods *5*, 61–67.

Kobat, D., Durst, M.E., Nishimura, N., Wong, A.W., Schaffer, C.B., and Xu, C. (2009). Deep tissue multiphoton microscopy using longer wavelength excitation. Opt. Express *17*, 13354–13364.

Koester, H.J., and Sakmann, B. (1998). Calcium dynamics in single spines during coincident pre- and postsynaptic activity depend on relative timing of back-propagating action potentials and subthreshold excitatory postsynaptic potentials. Proc. Natl. Acad. Sci. USA *95*, 9596–9601.

Koester, H.J., and Sakmann, B. (2000). Calcium dynamics associated with action potentials in single nerve terminals of pyramidal cells in layer 2/3 of the young rat neocortex. J. Physiol. *529*, 625–646.

Koh, D.S., Burnashev, N., and Jonas, P. (1995). Block of native Ca(2+)-permeable AMPA receptors in rat brain by intracellular polyamines generates double rectification. J. Physiol. *486*, 305–312.

Komiyama, T., Sato, T.R., O'Connor, D.H., Zhang, Y.X., Huber, D., Hooks, B.M., Gabitto, M., and Svoboda, K. (2010). Learning-related fine-scale specificity imaged in motor cortex circuits of behaving mice. Nature *464*, 1182–1186.

Konnerth, A., Dreessen, J., and Augustine, G.J. (1992). Brief dendritic calcium signals initiate long-lasting synaptic depression in cerebellar Purkinje cells. Proc. Natl. Acad. Sci. USA *89*, 7051–7055.

Kotlikoff, M.I. (2007). Genetically encoded Ca^{2+} indicators: using genetics and molecular design to understand complex physiology. J. Physiol. *578*, 55–67.

Kovalchuk, Y., Eilers, J., Lisman, J., and Konnerth, A. (2000). NMDA receptor-mediated subthreshold Ca(2+) signals in spines of hippocampal neurons. J. Neurosci. *20*, 1791–1799.

Kozloski, J., Hamzei-Sichani, F., and Yuste, R. (2001). Stereotyped position of local synaptic targets in neocortex. Science *293*, 868–872.

Kreile, A.K., Bonhoeffer, T., and Hübener, M. (2011). Altered visual experience induces instructive changes of orientation preference in mouse visual cortex. J. Neurosci. *31*, 13911–13920.

Kreitzer, A.C., Gee, K.R., Archer, E.A., and Regehr, W.G. (2000). Monitoring presynaptic calcium dynamics in projection fibers by in vivo loading of a novel calcium indicator. Neuron *27*, 25–32.

Kumar, M., Keller, B., Makalou, N., and Sutton, R.E. (2001). Systematic determination of the packaging limit of lentiviral vectors. Hum. Gene Ther. *12*, 1893–1905.

Langevin, L.M., Mattar, P., Scardigli, R., Roussigné, M., Logan, C., Blader, P., and Schuurmans, C. (2007). Validating in utero electroporation for the rapid analysis of gene regulatory elements in the murine telencephalon. Dev. Dyn. *236*, 1273–1286.

Larkum, M.E., Watanabe, S., Nakamura, T., Lasser-Ross, N., and Ross, W.N. (2003). Synaptically activated Ca^{2+} waves in layer 2/3 and layer 5 rat neocortical pyramidal neurons. J. Physiol. *549*, 471–488.

Lasser-Ross, N., Miyakawa, H., Lev-Ram, V., Young, S.R., and Ross, W.N. (1991). High time resolution fluorescence imaging with a CCD camera. J. Neurosci. Methods *36*, 253–261.

LeChasseur, Y., Dufour, S., Lavertu, G., Bories, C., Deschênes, M., Vallée, R., and De Koninck, Y. (2011). A microprobe for parallel optical and electrical recordings from single neurons in vivo. Nat. Methods *8*, 319–325.

Lechleiter, J.D., Lin, D.T., and Sieneart, I. (2002). Multi-photon laser scanning microscopy using an acoustic optical deflector. Biophys. J. *83*, 2292–2299.

Levene, M.J., Dombeck, D.A., Kasischke, K.A., Molloy, R.P., and Webb, W.W. (2004). In vivo multiphoton microscopy of deep brain tissue. J. Neurophysiol. *91*, 1908–1912.

Li, J., Mack, J.A., Souren, M., Yaksi, E., Higashijima, S., Mione, M., Fetcho, J.R., and Friedrich, R.W. (2005). Early development of functional spatial maps in the zebrafish olfactory bulb. J. Neurosci. *25*, 5784–5795.

Li, Y., Van Hooser, S.D., Mazurek, M., White, L.E., and Fitzpatrick, D. (2008). Experience with moving visual stimuli drives the early development of cortical direction selectivity. Nature *456*, 952–956.

Lichtman, J.W., and Conchello, J.A. (2005). Fluorescence microscopy. Nat. Methods *2*, 910–919.

Lilley, C.E., Groutsi, F., Han, Z., Palmer, J.A., Anderson, P.N., Latchman, D.S., and Coffin, R.S. (2001). Multiple immediate-early gene-deficient herpes simplex virus vectors allowing efficient gene delivery to neurons in culture and widespread gene delivery to the central nervous system in vivo. J. Virol. *75*, 4343–4356.

Liu, S.J., and Zukin, R.S. (2007). Ca^{2+}-permeable AMPA receptors in synaptic plasticity and neuronal death. Trends Neurosci. *30*, 126–134.

Liu, S.Q., and Cull-Candy, S.G. (2000). Synaptic activity at calcium-permeable AMPA receptors induces a switch in receptor subtype. Nature *405*, 454–458.

Llano, I., González, J., Caputo, C., Lai, F.A., Blayney, L.M., Tan, Y.P., and Marty, A. (2000). Presynaptic calcium stores underlie large-amplitude miniature IPSCs and spontaneous calcium transients. Nat. Neurosci. *3*, 1256–1265.

Llinás, R., and Nicholson, C. (1975). Calcium role in depolarization-secretion coupling: an aequorin study in squid giant synapse. Proc. Natl. Acad. Sci. USA *72*, 187–190.

Lohmann, C., Finski, A., and Bonhoeffer, T. (2005). Local calcium transients regulate the spontaneous motility of dendritic filopodia. Nat. Neurosci. *8*, 305–312.

Looger, L.L., and Griesbeck, O. (2011). Genetically encoded neural activity indicators. Curr. Opin. Neurobiol., in press. Published online November 19, 2011.

Lu, K.P., and Means, A.R. (1993). Regulation of the cell cycle by calcium and calmodulin. Endocr. Rev. *14*, 40–58.

Luo, L., Callaway, E.M., and Svoboda, K. (2008). Genetic dissection of neural circuits. Neuron *57*, 634–660.

Lüscher, C., and Huber, K.M. (2010). Group 1 mGluR-dependent synaptic long-term depression: mechanisms and implications for circuitry and disease. Neuron *65*, 445–459.

Lütcke, H., Murayama, M., Hahn, T., Margolis, D.J., Astori, S., Zum Alten Borgloh, S.M., Göbel, W., Yang, Y., Tang, W., Kügler, S., et al. (2010). Optical recording of neuronal activity with a genetically-encoded calcium indicator in anesthetized and freely moving mice. Front Neural Circuits *4*, 9.

Lyons, M.R., and West, A.E. (2011). Mechanisms of specificity in neuronal activity-regulated gene transcription. Prog. Neurobiol. *94*, 259–295.

Mahanty, N.K., and Sah, P. (1998). Calcium-permeable AMPA receptors mediate long-term potentiation in interneurons in the amygdala. Nature *394*, 683–687.

Manita, S., and Ross, W.N. (2009). Synaptic activation and membrane potential changes modulate the frequency of spontaneous elementary Ca2+ release events in the dendrites of pyramidal neurons. J. Neurosci. *29*, 7833–7845.

Mank, M., and Griesbeck, O. (2008). Genetically encoded calcium indicators. Chem. Rev. *108*, 1550–1564.

Mank, M., Reiff, D.F., Heim, N., Friedrich, M.W., Borst, A., and Griesbeck, O. (2006). A FRET-based calcium biosensor with fast signal kinetics and high fluorescence change. Biophys. J. *90*, 1790–1796.

Mank, M., Santos, A.F., Direnberger, S., Mrsic-Flogel, T.D., Hofer, S.B., Stein, V., Hendel, T., Reiff, D.F., Levelt, C., Borst, A., et al. (2008). A genetically encoded calcium indicator for chronic in vivo two-photon imaging. Nat. Methods *5*, 805–811.

Mao, B.Q., Hamzei-Sichani, F., Aronov, D., Froemke, R.C., and Yuste, R. (2001). Dynamics of spontaneous activity in neocortical slices. Neuron *32*, 883–898.

Mao, T., O'Connor, D.H., Scheuss, V., Nakai, J., and Svoboda, K. (2008). Characterization and subcellular targeting of GCaMP-type genetically-encoded calcium indicators. PLoS ONE *3*, e1796.

Margrie, T.W., Brecht, M., and Sakmann, B. (2002). In vivo, low-resistance, whole-cell recordings from neurons in the anaesthetized and awake mammalian brain. Pflugers Arch. *444*, 491–498.

Margrie, T.W., Meyer, A.H., Caputi, A., Monyer, H., Hasan, M.T., Schaefer, A.T., Denk, W., and Brecht, M. (2003). Targeted whole-cell recordings in the mammalian brain in vivo. Neuron *39*, 911–918.

Martin, J.R., Rogers, K.L., Chagneau, C., and Brûlet, P. (2007). In vivo bioluminescence imaging of Ca signalling in the brain of Drosophila. PLoS ONE *2*, e275.

Mayer, M.L., Westbrook, G.L., and Guthrie, P.B. (1984). Voltage-dependent block by Mg^{2+} of NMDA responses in spinal cord neurones. Nature *309*, 261–263.

Minderer, M., Liu, W., Sumanovski, L.T., Kügler, S., Helmchen, F., and Margolis, D.J. (2012). Chronic imaging of cortical sensory map dynamics using a genetically encoded calcium indicator. J. Physiol. *590*, 99–107.

Mittmann, W., Wallace, D.J., Czubayko, U., Herb, J.T., Schaefer, A.T., Looger, L.L., Denk, W., and Kerr, J.N. (2011). Two-photon calcium imaging of evoked activity from L5 somatosensory neurons in vivo. Nat. Neurosci. *14*, 1089–1093.

Miyawaki, A., Griesbeck, O., Heim, R., and Tsien, R.Y. (1999). Dynamic and quantitative Ca^{2+} measurements using improved cameleons. Proc. Natl. Acad. Sci. USA *96*, 2135–2140.

Miyawaki, A., Llopis, J., Heim, R., McCaffery, J.M., Adams, J.A., Ikura, M., and Tsien, R.Y. (1997). Fluorescent indicators for Ca^{2+} based on green fluorescent proteins and calmodulin. Nature *388*, 882–887.

Mizrahi, A., Crowley, J.C., Shtoyerman, E., and Katz, L.C. (2004). High-resolution in vivo imaging of hippocampal dendrites and spines. J. Neurosci. *24*, 3147–3151.

Monahan, P.E., and Samulski, R.J. (2000). Adeno-associated virus vectors for gene therapy: more pros than cons? Mol. Med. Today *6*, 433–440.

Mrsic-Flogel, T.D., Hofer, S.B., Ohki, K., Reid, R.C., Bonhoeffer, T., and Hübener, M. (2007). Homeostatic regulation of eye-specific responses in visual cortex during ocular dominance plasticity. Neuron *54*, 961–972.

Murayama, M., and Larkum, M.E. (2009). In vivo dendritic calcium imaging with a fiberoptic periscope system. Nat. Protoc. *4*, 1551–1559.

Murayama, M., Pérez-Garci, E., Lüscher, H.R., and Larkum, M.E. (2007). Fiberoptic system for recording dendritic calcium signals in layer 5 neocortical pyramidal cells in freely moving rats. J. Neurophysiol. *98*, 1791–1805.

Murayama, M., Pérez-Garci, E., Nevian, T., Bock, T., Senn, W., and Larkum, M.E. (2009). Dendritic encoding of sensory stimuli controlled by deep cortical interneurons. Nature *457*, 1137–1141.

Nagai, T., Sawano, A., Park, E.S., and Miyawaki, A. (2001). Circularly permuted green fluorescent proteins engineered to sense Ca2+. Proc. Natl. Acad. Sci. USA *98*, 3197–3202.

Nagai, T., Yamada, S., Tominaga, T., Ichikawa, M., and Miyawaki, A. (2004). Expanded dynamic range of fluorescent indicators for $Ca^{(2+)}$ by circularly permuted yellow fluorescent proteins. Proc. Natl. Acad. Sci. USA *101*, 10554–10559.

Nagayama, S., Enerva, A., Fletcher, M.L., Masurkar, A.V., Igarashi, K.M., Mori, K., and Chen, W.R. (2010). Differential axonal projection of mitral and tufted cells in the mouse main olfactory system. Front Neural Circuits *4*, 120.

Nagayama, S., Zeng, S., Xiong, W., Fletcher, M.L., Masurkar, A.V., Davis, D.J., Pieribone, V.A., and Chen, W.R. (2007). In vivo simultaneous tracing and $Ca^{(2+)}$ imaging of local neuronal circuits. Neuron *53*, 789–803.

Nakai, J., Ohkura, M., and Imoto, K. (2001). A high signal-to-noise $Ca^{(2+)}$ probe composed of a single green fluorescent protein. Nat. Biotechnol. *19*, 137–141.

Nakamura, T., Barbara, J.G., Nakamura, K., and Ross, W.N. (1999). Synergistic release of Ca^{2+} from IP_3-sensitive stores evoked by synaptic activation of mGluRs paired with backpropagating action potentials. Neuron *24*, 727–737.

Nathanson, J.L., Jappelli, R., Scheeff, E.D., Manning, G., Obata, K., Brenner, S., and Callaway, E.M. (2009a). Short Promoters in Viral Vectors Drive Selective Expression in Mammalian Inhibitory Neurons, but do not Restrict Activity to Specific Inhibitory Cell-Types. Front Neural Circuits *3*, 19.

Nathanson, J.L., Yanagawa, Y., Obata, K., and Callaway, E.M. (2009b). Preferential labeling of inhibitory and excitatory cortical neurons by endogenous tropism of adeno-associated virus and lentivirus vectors. Neuroscience *161*, 441–450.

Neher, E. (1995). The use of fura-2 for estimating Ca buffers and Ca fluxes. Neuropharmacology *34*, 1423–1442.

Neher, E., and Augustine, G.J. (1992). Calcium gradients and buffers in bovine chromaffin cells. J. Physiol. *450*, 273–301.

Neher, E., and Sakaba, T. (2008). Multiple roles of calcium ions in the regulation of neurotransmitter release. Neuron *59*, 861–872.

Nevian, T., and Helmchen, F. (2007). Calcium indicator loading of neurons using single-cell electroporation. Pflugers Arch. *454*, 675–688.

Nevian, T., and Sakmann, B. (2006). Spine Ca^{2+} signaling in spike-timing-dependent plasticity. J. Neurosci. *26*, 11001–11013.

Nguyen, Q.T., Callamaras, N., Hsieh, C., and Parker, I. (2001). Construction of a two-photon microscope for video-rate $Ca^{(2+)}$ imaging. Cell Calcium *30*, 383–393.

Nimmerjahn, A., Kirchhoff, F., Kerr, J.N., and Helmchen, F. (2004). Sulforhodamine 101 as a specific marker of astroglia in the neocortex in vivo. Nat. Methods *1*, 31–37.

Niswender, C.M., and Conn, P.J. (2010). Metabotropic glutamate receptors: physiology, pharmacology, and disease. Annu. Rev. Pharmacol. Toxicol. *50*, 295–322.

Nowak, L., Bregestovski, P., Ascher, P., Herbet, A., and Prochiantz, A. (1984). Magnesium gates glutamate-activated channels in mouse central neurones. Nature *307*, 462–465.

O'Donovan, M.J., Bonnot, A., Wenner, P., and Mentis, G.Z. (2005). Calcium imaging of network function in the developing spinal cord. Cell Calcium *37*, 443–450.

Oheim, M., Beaurepaire, E., Chaigneau, E., Mertz, J., and Charpak, S. (2001). Two-photon microscopy in brain tissue: parameters influencing the imaging depth. J. Neurosci. Methods *111*, 29–37.

Ohki, K., Chung, S., Ch'ng, Y.H., Kara, P., and Reid, R.C. (2005). Functional imaging with cellular resolution reveals precise micro-architecture in visual cortex. Nature *433*, 597–603.

Ohki, K., Chung, S., Kara, P., Hübener, M., Bonhoeffer, T., and Reid, R.C. (2006). Highly ordered arrangement of single neurons in orientation pinwheels. Nature *442*, 925–928.

Ohmiya, Y., and Hirano, T. (1996). Shining the light: the mechanism of the bioluminescence reaction of calcium-binding photoproteins. Chem. Biol. *3*, 337–347.

Oka, Y., Katada, S., Omura, M., Suwa, M., Yoshihara, Y., and Touhara, K. (2006). Odorant receptor map in the mouse olfactory bulb: in vivo sensitivity and specificity of receptor-defined glomeruli. Neuron *52*, 857–869.

Oliver, A.E., Baker, G.A., Fugate, R.D., Tablin, F., and Crowe, J.H. (2000). Effects of temperature on calcium-sensitive fluorescent probes. Biophys. J. *78*, 2116–2126.

Orrenius, S., Zhivotovsky, B., and Nicotera, P. (2003). Regulation of cell death: the calcium-apoptosis link. Nat. Rev. Mol. Cell Biol. *4*, 552–565.

Osakada, F., Mori, T., Cetin, A.H., Marshel, J.H., Virgen, B., and Callaway, E.M. (2011). New rabies virus variants for monitoring and manipulating activity and gene expression in defined neural circuits. Neuron *71*, 617–631.

Otsu, Y., Bormuth, V., Wong, J., Mathieu, B., Dugué, G.P., Feltz, A., and Dieudonné, S. (2008). Optical monitoring of neuronal activity at high frame rate with a digital random-access multiphoton (RAMP) microscope. J. Neurosci. Methods *173*, 259–270.

Palmer, A.E., Giacomello, M., Kortemme, T., Hires, S.A., Lev-Ram, V., Baker, D., and Tsien, R.Y. (2006). Ca^{2+} indicators based on computationally redesigned calmodulin-peptide pairs. Chem. Biol. *13*, 521–530.

Paredes, R.M., Etzler, J.C., Watts, L.T., Zheng, W., and Lechleiter, J.D. (2008). Chemical calcium indicators. Methods *46*, 143–151.

Plant, T.D., Schirra, C., Katz, E., Uchitel, O.D., and Konnerth, A. (1998). Single-cell RT-PCR and functional characterization of Ca^{2+} channels in motoneurons of the rat facial nucleus. J. Neurosci. *18*, 9573–9584.

Pologruto, T.A., Yasuda, R., and Svoboda, K. (2004). Monitoring neural activity and [Ca^{2+}] with genetically encoded Ca^{2+} indicators. J. Neurosci. *24*, 9572–9579.

Pozzan, T., Arslan, P., Tsien, R.Y., and Rink, T.J. (1982). Anti-immunoglobulin, cytoplasmic free calcium, and capping in B lymphocytes. J. Cell Biol. *94*, 335–340.

Ramsey, I.S., Delling, M., and Clapham, D.E. (2006). An introduction to TRP channels. Annu. Rev. Physiol. *68*, 619–647.

Ravin, R., Spira, M.E., Parnas, H., and Parnas, I. (1997). Simultaneous measurement of intracellular Ca^{2+} and asynchronous transmitter release from the same crayfish bouton. J. Physiol. *501*, 251–262.

Raymond, C.R., and Redman, S.J. (2006). Spatial segregation of neuronal calcium signals encodes different forms of LTP in rat hippocampus. J. Physiol. *570*, 97–111.

Regehr, W.G., and Tank, D.W. (1991a). The maintenance of LTP at hippocampal mossy fiber synapses is independent of sustained presynaptic calcium. Neuron *7*, 451–459.

Regehr, W.G., and Tank, D.W. (1991b). Selective fura-2 loading of presynaptic terminals and nerve cell processes by local perfusion in mammalian brain slice. J. Neurosci. Methods *37*, 111–119.

Regehr, W.G., and Tank, D.W. (1994). Dendritic calcium dynamics. Curr. Opin. Neurobiol. *4*, 373–382.

Reid, C.A., Fabian-Fine, R., and Fine, A. (2001). Postsynaptic calcium transients evoked by activation of individual hippocampal mossy fiber synapses. J. Neurosci. *21*, 2206–2214.

Rizzuto, R., and Pozzan, T. (2006). Microdomains of intracellular Ca^{2+}: molecular determinants and functional consequences. Physiol. Rev. *86*, 369–408.

Rizzuto, R., Simpson, A.W., Brini, M., and Pozzan, T. (1992). Rapid changes of mitochondrial Ca^{2+} revealed by specifically targeted recombinant aequorin. Nature *358*, 325–327.

Rochefort, N.L., Garaschuk, O., Milos, R.I., Narushima, M., Marandi, N., Pichler, B., Kovalchuk, Y., and Konnerth, A. (2009). Sparsification of neuronal activity in the visual cortex at eye-opening. Proc. Natl. Acad. Sci. USA *106*, 15049–15054.

Rochefort, N.L., Jia, H., and Konnerth, A. (2008). Calcium imaging in the living brain: prospects for molecular medicine. Trends Mol. Med. *14*, 389–399.

Rochefort, N.L., Narushima, M., Grienberger, C., Marandi, N., Hill, D.N., and Konnerth, A. (2011). Development of direction selectivity in mouse cortical neurons. Neuron *71*, 425–432.

Rogers, K.L., Stinnakre, J., Agulhon, C., Jublot, D., Shorte, S.L., Kremer, E.J., and Brûlet, P. (2005). Visualization of local Ca^{2+} dynamics with genetically encoded bioluminescent reporters. Eur. J. Neurosci. *21*, 597–610.

Rogers, M., and Dani, J.A. (1995). Comparison of quantitative calcium flux through NMDA, ATP, and ACh receptor channels. Biophys. J. *68*, 501–506.

Ross, W.N., and Werman, R. (1987). Mapping calcium transients in the dendrites of Purkinje cells from the guinea-pig cerebellum in vitro. J. Physiol. *389*, 319–336.

Rothschild, G., Nelken, I., and Mizrahi, A. (2010). Functional organization and population dynamics in the mouse primary auditory cortex. Nat. Neurosci. *13*, 353–360.

Rueckel, M., Mack-Bucher, J.A., and Denk, W. (2006). Adaptive wavefront correction in two-photon microscopy using coherence-gated wavefront sensing. Proc. Natl. Acad. Sci. USA *103*, 17137–17142.

Runyan, C.A., Schummers, J., Van Wart, A., Kuhlman, S.J., Wilson, N.R., Huang, Z.J., and Sur, M. (2010). Response features of parvalbumin-expressing interneurons suggest precise roles for subtypes of inhibition in visual cortex. Neuron *67*, 847–857.

Rusakov, D.A., Wuerz, A., and Kullmann, D.M. (2004). Heterogeneity and specificity of presynaptic Ca^{2+} current modulation by mGluRs at individual hippocampal synapses. Cereb. Cortex *14*, 748–758.

Sabatini, B.L., Oertner, T.G., and Svoboda, K. (2002). The life cycle of $Ca^{(2+)}$ ions in dendritic spines. Neuron *33*, 439–452.

Sasaki, T., Takahashi, N., Matsuki, N., and Ikegaya, Y. (2008). Fast and accurate detection of action potentials from somatic calcium fluctuations. J. Neurophysiol. *100*, 1668–1676.

Sato, T.R., Gray, N.W., Mainen, Z.F., and Svoboda, K. (2007). The functional microarchitecture of the mouse barrel cortex. PLoS Biol. *5*, e189.

Sawinski, J., Wallace, D.J., Greenberg, D.S., Grossmann, S., Denk, W., and Kerr, J.N. (2009). Visually evoked activity in cortical cells imaged in freely moving animals. Proc. Natl. Acad. Sci. USA *106*, 19557–19562.

Schneggenburger, R., Zhou, Z., Konnerth, A., and Neher, E. (1993). Fractional contribution of calcium to the cation current through glutamate receptor channels. Neuron *11*, 133–143.

Schwaller, B. (2010). Cytosolic Ca^{2+} buffers. Cold Spring Harb Perspect Biol *2*, a004051.

Seelig, J.D., Chiappe, M.E., Lott, G.K., Dutta, A., Osborne, J.E., Reiser, M.B., and Jayaraman, V. (2010). Two-photon calcium imaging from head-fixed Drosophila during optomotor walking behavior. Nat. Methods *7*, 535–540.

Segal, M. (1995). Fast imaging of [Ca]i reveals presence of voltage-gated calcium channels in dendritic spines of cultured hippocampal neurons. J. Neurophysiol. *74*, 484–488.

Sherman, L., Ye, J.Y., Albert, O., and Norris, T.B. (2002). Adaptive correction of depth-induced aberrations in multiphoton scanning microscopy using a deformable mirror. J. Microsc. *206*, 65–71.

Shevtsova, Z., Malik, J.M., Michel, U., Bähr, M., and Kügler, S. (2005). Promoters and serotypes: targeting of adeno-associated virus vectors for gene transfer in the rat central nervous system in vitro and in vivo. Exp. Physiol. *90*, 53–59.

Shigetomi, E., Kracun, S., Sofroniew, M.V., and Khakh, B.S. (2010). A genetically targeted optical sensor to monitor calcium signals in astrocyte processes. Nat. Neurosci. *13*, 759–766.

Shimogori, T., and Ogawa, M. (2008). Gene application with in utero electroporation in mouse embryonic brain. Dev. Growth Differ. *50*, 499–506.

Shimomura, O. (1997). Membrane permeability of coelenterazine analogues measured with fish eggs. Biochem. J. *326*, 297–298.

Shimomura, O., Johnson, F.H., and Saiga, Y. (1962). Extraction, purification and properties of aequorin, a bioluminescent protein from the luminous hydromedusan, Aequorea. J. Cell. Comp. Physiol. *59*, 223–239.

Shimomura, O., Kishi, Y., and Inouye, S. (1993). The relative rate of aequorin regeneration from apoaequorin and coelenterazine analogues. Biochem. J. *296*, 549–551.

Skeberdis, V.A., Chevaleyre, V., Lau, C.G., Goldberg, J.H., Pettit, D.L., Suadicani, S.O., Lin, Y., Bennett, M.V., Yuste, R., Castillo, P.E., and Zukin, R.S. (2006). Protein kinase A regulates calcium permeability of NMDA receptors. Nat. Neurosci. *9*, 501–510.

Smith, S.J., and Augustine, G.J. (1988). Calcium ions, active zones and synaptic transmitter release. Trends Neurosci. *11*, 458–464.

Smith, S.J., Buchanan, J., Osses, L.R., Charlton, M.P., and Augustine, G.J. (1993). The spatial distribution of calcium signals in squid presynaptic terminals. J. Physiol. *472*, 573–593.

Smith, S.L., and Häusser, M. (2010). Parallel processing of visual space by neighboring neurons in mouse visual cortex. Nat. Neurosci. *13*, 1144–1149.

Sobczyk, A., Scheuss, V., and Svoboda, K. (2005). NMDA receptor subunit-dependent [Ca^{2+}] signaling in individual hippocampal dendritic spines. J. Neurosci. *25*, 6037–6046.

Sobczyk, A., and Svoboda, K. (2007). Activity-dependent plasticity of the NMDA-receptor fractional Ca^{2+} current. Neuron *53*, 17–24.

Sohya, K., Kameyama, K., Yanagawa, Y., Obata, K., and Tsumoto, T. (2007). GABAergic neurons are less selective to stimulus orientation than excitatory neurons in layer II/III of visual cortex, as revealed by in vivo functional Ca^{2+} imaging in transgenic mice. J. Neurosci. *27*, 2145–2149.

Soudais, C., Skander, N., and Kremer, E.J. (2004). Long-term in vivo transduction of neurons throughout the rat CNS using novel helper-dependent CAV-2 vectors. FASEB J. *18*, 391–393.

Spruston, N., Schiller, Y., Stuart, G., and Sakmann, B. (1995). Activity-dependent action potential invasion and calcium influx into hippocampal CA1 dendrites. Science *268*, 297–300.

Stephens, D.J., and Allan, V.J. (2003). Light microscopy techniques for live cell imaging. Science *300*, 82–86.

Stinnakre, J., and Tauc, L. (1973). Calcium influx in active Aplysia neurones detected by injected aequorin. Nat. New Biol. *242*, 113–115.

Stosiek, C., Garaschuk, O., Holthoff, K., and Konnerth, A. (2003). In vivo two-photon calcium imaging of neuronal networks. Proc. Natl. Acad. Sci. USA *100*, 7319–7324.

Sullivan, M.R., Nimmerjahn, A., Sarkisov, D.V., Helmchen, F., and Wang, S.S. (2005). In vivo calcium imaging of circuit activity in cerebellar cortex. J. Neurophysiol. *94*, 1636–1644.

Sumbre, G., Muto, A., Baier, H., and Poo, M.M. (2008). Entrained rhythmic activities of neuronal ensembles as perceptual memory of time interval. Nature *456*, 102–106.

Svoboda, K., Denk, W., Kleinfeld, D., and Tank, D.W. (1997). In vivo dendritic calcium dynamics in neocortical pyramidal neurons. Nature *385*, 161–165.

Svoboda, K., Helmchen, F., Denk, W., and Tank, D.W. (1999). Spread of dendritic excitation in layer 2/3 pyramidal neurons in rat barrel cortex in vivo. Nat. Neurosci. *2*, 65–73.

Svoboda, K., and Yasuda, R. (2006). Principles of two-photon excitation microscopy and its applications to neuroscience. Neuron *50*, 823–839.

Swandulla, D., Hans, M., Zipser, K., and Augustine, G.J. (1991). Role of residual calcium in synaptic depression and posttetanic potentiation: fast and slow calcium signaling in nerve terminals. Neuron *7*, 915–926.

Tabata, H., and Nakajima, K. (2001). Efficient in utero gene transfer system to the developing mouse brain using electroporation: visualization of neuronal migration in the developing cortex. Neuroscience *103*, 865–872.

Takahara, Y., Matsuki, N., and Ikegaya, Y. (2011). Nipkow confocal imaging from deep brain tissues. J. Integr. Neurosci. *10*, 121–129.

Takahashi, N., Kitamura, K., Matsuo, N., Mayford, M., Kano, M., Matsuki, N., and Ikegaya, Y. (2012). Locally synchronized synaptic inputs. Science *335*, 353–356.

Takano, T., Tian, G.F., Peng, W., Lou, N., Libionka, W., Han, X., and Nedergaard, M. (2006). Astrocyte-mediated control of cerebral blood flow. Nat. Neurosci. *9*, 260–267.

Takechi, H., Eilers, J., and Konnerth, A. (1998). A new class of synaptic response involving calcium release in dendritic spines. Nature *396*, 757–760.

Tamamaki, N., Yanagawa, Y., Tomioka, R., Miyazaki, J., Obata, K., and Kaneko, T. (2003). Green fluorescent protein expression and colocalization with calretinin, parvalbumin, and somatostatin in the GAD67-GFP knock-in mouse. J. Comp. Neurol. *467*, 60–79.

Tao, H.W., Zhang, L.I., Engert, F., and Poo, M. (2001). Emergence of input specificity of ltp during development of retinotectal connections in vivo. Neuron *31*, 569–580.

Theer, P., Hasan, M.T., and Denk, W. (2003). Two-photon imaging to a depth of 1000 microm in living brains by use of a Ti:Al2O3 regenerative amplifier. Opt. Lett. *28*, 1022–1024.

Tian, L., Hires, S.A., Mao, T., Huber, D., Chiappe, M.E., Chalasani, S.H., Petreanu, L., Akerboom, J., McKinney, S.A., Schreiter, E.R., et al. (2009). Imaging neural activity in worms, flies and mice with improved GCaMP calcium indicators. Nat. Methods *6*, 875–881.

Tóth, K., and McBain, C.J. (1998). Afferent-specific innervation of two distinct AMPA receptor subtypes on single hippocampal interneurons. Nat. Neurosci. *1*, 572–578.

Trevelyan, A.J., Sussillo, D., Watson, B.O., and Yuste, R. (2006). Modular propagation of epileptiform activity: evidence for an inhibitory veto in neocortex. J. Neurosci. *26*, 12447–12455.

Tsai, P.S., Friedman, B., Ifarraguerri, A.I., Thompson, B.D., Lev-Ram, V., Schaffer, C.B., Xiong, Q., Tsien, R.Y., Squier, J.A., and Kleinfeld, D. (2003). All-optical histology using ultrashort laser pulses. Neuron *39*, 27–41.

Tsien, R.Y. (1980). New calcium indicators and buffers with high selectivity against magnesium and protons: design, synthesis, and properties of prototype structures. Biochemistry *19*, 2396–2404.

Tsien, R.Y. (1981). A non-disruptive technique for loading calcium buffers and indicators into cells. Nature *290*, 527–528.

Tsien, R.Y. (1989). Fluorescent probes of cell signaling. Annu. Rev. Neurosci. *12*, 227–253.

Tsien, R.W., and Tsien, R.Y. (1990). Calcium channels, stores, and oscillations. Annu. Rev. Cell Biol. *6*, 715–760.

Tsien, R.Y., Pozzan, T., and Rink, T.J. (1982). Calcium homeostasis in intact lymphocytes: cytoplasmic free calcium monitored with a new, intracellularly trapped fluorescent indicator. J. Cell Biol. *94*, 325–334.

Tsien, R.Y., Rink, T.J., and Poenie, M. (1985). Measurement of cytosolic free Ca^{2+} in individual small cells using fluorescence microscopy with dual excitation wavelengths. Cell Calcium *6*, 145–157.

Usowicz, M.M., Sugimori, M., Cherksey, B., and Llinás, R. (1992). P-type calcium channels in the somata and dendrites of adult cerebellar Purkinje cells. Neuron *9*, 1185–1199.

Varga, Z., Jia, H., Sakmann, B., and Konnerth, A. (2011). Dendritic coding of multiple sensory inputs in single cortical neurons in vivo. Proc. Natl. Acad. Sci. USA *108*, 15420–15425.

Vogelstein, J.T., Packer, A.M., Machado, T.A., Sippy, T., Babadi, B., Yuste, R., and Paninski, L. (2010). Fast nonnegative deconvolution for spike train inference from population calcium imaging. J. Neurophysiol. *104*, 3691–3704.

Vogelstein, J.T., Watson, B.O., Packer, A.M., Yuste, R., Jedynak, B., and Paninski, L. (2009). Spike inference from calcium imaging using sequential Monte Carlo methods. Biophys. J. *97*, 636–655.

Wachowiak, M., and Cohen, L.B. (2001). Representation of odorants by receptor neuron input to the mouse olfactory bulb. Neuron *32*, 723–735.

Wachowiak, M., Cohen, L.B., and Zochowski, M.R. (2002). Distributed and concentration-invariant spatial representations of odorants by receptor neuron input to the turtle olfactory bulb. J. Neurophysiol. *87*, 1035–1045.

Wachowiak, M., Denk, W., and Friedrich, R.W. (2004). Functional organization of sensory input to the olfactory bulb glomerulus analyzed by two-photon calcium imaging. Proc. Natl. Acad. Sci. USA *101*, 9097–9102.

Wallace, D.J., Meyer zum Alten Borgloh, S., Astori, S., Yang, Y., Bausen, M., Kügler, S., Palmer, A.E., Tsien, R.Y., Sprengel, R., Kerr, J.N., et al. (2008). Single-spike detection in vitro and in vivo with a genetic Ca^{2+} sensor. Nat. Methods *5*, 797–804.

Wang, J.W., Wong, A.M., Flores, J., Vosshall, L.B., and Axel, R. (2003). Two-photon calcium imaging reveals an odor-evoked map of activity in the fly brain. Cell *112*, 271–282.

Wang, S.S., Denk, W., and Häusser, M. (2000). Coincidence detection in single dendritic spines mediated by calcium release. Nat. Neurosci. *3*, 1266–1273.

Wang, X., Lou, N., Xu, Q., Tian, G.F., Peng, W.G., Han, X., Kang, J., Takano, T., and Nedergaard, M. (2006). Astrocytic Ca^{2+} signaling evoked by sensory stimulation in vivo. Nat. Neurosci. *9*, 816–823.

Waters, J., and Helmchen, F. (2004). Boosting of action potential backpropagation by neocortical network activity in vivo. J. Neurosci. *24*, 11127–11136.

Waters, J., Larkum, M., Sakmann, B., and Helmchen, F. (2003). Supralinear Ca^{2+} influx into dendritic tufts of layer 2/3 neocortical pyramidal neurons in vitro and in vivo. J. Neurosci. *23*, 8558–8567.

Waters, J., Schaefer, A., and Sakmann, B. (2005). Backpropagating action potentials in neurones: measurement, mechanisms and potential functions. Prog. Biophys. Mol. Biol. *87*, 145–170.

Wettschureck, N., and Offermanns, S. (2005). Mammalian G proteins and their cell type specific functions. Physiol. Rev. *85*, 1159–1204.

Wilson, T. (2010). Spinning-disk microscopy systems. Cold Spring Harb Protoc *2010*, pdb.top88.

Wilt, B.A., Burns, L.D., Wei Ho, E.T., Ghosh, K.K., Mukamel, E.A., and Schnitzer, M.J. (2009). Advances in light microscopy for neuroscience. Annu. Rev. Neurosci. *32*, 435–506.

Winship, I.R., and Murphy, T.H. (2008). In vivo calcium imaging reveals functional rewiring of single somatosensory neurons after stroke. J. Neurosci. *28*, 6592–6606.

Wirth, D., Gama-Norton, L., Riemer, P., Sandhu, U., Schucht, R., and Hauser, H. (2007). Road to precision: recombinase-based targeting technologies for genome engineering. Curr. Opin. Biotechnol. *18*, 411–419.

Witten, I.B., Steinberg, E.E., Lee, S.Y., Davidson, T.J., Zalocusky, K.A., Brodsky, M., Yizhar, O., Cho, S.L., Gong, S., Ramakrishnan, C., et al. (2011). Recombinase-driver rat lines: tools, techniques, and optogenetic application to dopamine-mediated reinforcement. Neuron *72*, 721–733.

Wokosin, D.L., Loughrey, C.M., and Smith, G.L. (2004). Characterization of a range of fura dyes with two-photon excitation. Biophys. J. *86*, 1726–1738.

Xu, C., Zipfel, W., Shear, J.B., Williams, R.M., and Webb, W.W. (1996). Multiphoton fluorescence excitation: new spectral windows for biological nonlinear microscopy. Proc. Natl. Acad. Sci. USA *93*, 10763–10768.

Xu, X., Soutto, M., Xie, Q., Servick, S., Subramanian, C., von Arnim, A.G., and Johnson, C.H. (2007). Imaging protein interactions with bioluminescence resonance energy transfer (BRET) in plant and mammalian cells and tissues. Proc. Natl. Acad. Sci. USA *104*, 10264–10269.

Yaksi, E., and Friedrich, R.W. (2006). Reconstruction of firing rate changes across neuronal populations by temporally deconvolved Ca2+ imaging. Nat. Methods *3*, 377–383.

Yaksi, E., von Saint Paul, F., Niessing, J., Bundschuh, S.T., and Friedrich, R.W. (2009). Transformation of odor representations in target areas of the olfactory bulb. Nat. Neurosci. *12*, 474–482.

Yamada, Y., Michikawa, T., Hashimoto, M., Horikawa, K., Nagai, T., Miyawaki, A., Häusser, M., and Mikoshiba, K. (2011). Quantitative comparison of genetically encoded ca indicators in cortical pyramidal cells and cerebellar purkinje cells. Front Cell Neurosci *5*, 18.

Yang, G., Pan, F., Parkhurst, C.N., Grutzendler, J., and Gan, W.B. (2010). Thinned-skull cranial window technique for long-term imaging of the cortex in live mice. Nat. Protoc. *5*, 201–208.

Yasuda, R., Sabatini, B.L., and Svoboda, K. (2003). Plasticity of calcium channels in dendritic spines. Nat. Neurosci. *6*, 948–955.

Yizhar, O., Fenno, L.E., Davidson, T.J., Mogri, M., and Deisseroth, K. (2011). Optogenetics in neural systems. Neuron *71*, 9–34.

Yu, D., Baird, G.S., Tsien, R.Y., and Davis, R.L. (2003). Detection of calcium transients in Drosophila mushroom body neurons with camgaroo reporters. J. Neurosci. *23*, 64–72.

Yuste, R., and Denk, W. (1995). Dendritic spines as basic functional units of neuronal integration. Nature *375*, 682–684.

Yuste, R., and Katz, L.C. (1991). Control of postsynaptic Ca2+ influx in developing neocortex by excitatory and inhibitory neurotransmitters. Neuron *6*, 333–344.

Yuste, R., Majewska, A., Cash, S.S., and Denk, W. (1999). Mechanisms of calcium influx into hippocampal spines: heterogeneity among spines, coincidence detection by NMDA receptors, and optical quantal analysis. J. Neurosci. *19*, 1976–1987.

Yuste, R., Peinado, A., and Katz, L.C. (1992). Neuronal domains in developing neocortex. Science *257*, 665–669.

Zhang, F., Aravanis, A.M., Adamantidis, A., de Lecea, L., and Deisseroth, K. (2007). Circuit-breakers: optical technologies for probing neural signals and systems. Nat. Rev. Neurosci. *8*, 577–581.

Zhao, Y., Araki, S., Wu, J., Teramoto, T., Chang, Y.F., Nakano, M., Abdelfattah, A.S., Fujiwara, M., Ishihara, T., Nagai, T., and Campbell, R.E. (2011). An expanded palette of genetically encoded Ca^{2+} indicators. Science *333*, 1888–1891.

Zucker, R.S. (1999). Calcium- and activity-dependent synaptic plasticity. Curr. Opin. Neurobiol. *9*, 305–313.